


Spring 2018

# Biomimetic Studies of Oxidation Reactions by Metalloporphyrins through Ligand Effect and Kinetic Studies of Photo-Generated Porphyrin-Iron(IV)- Oxocompound II Models

Dharmesh J. Patel

Western Kentucky University, dharmeshj.patel086@topper.wku.edu

Follow this and additional works at: <https://digitalcommons.wku.edu/theses>

 Part of the [Biochemistry Commons](#), and the [Organic Chemistry Commons](#)

## Recommended Citation

Patel, Dharmesh J., "Biomimetic Studies of Oxidation Reactions by Metalloporphyrins through Ligand Effect and Kinetic Studies of Photo-Generated Porphyrin-Iron(IV)- Oxocompound II Models" (2018). *Masters Theses & Specialist Projects*. Paper 2091.  
<https://digitalcommons.wku.edu/theses/2091>

This Thesis is brought to you for free and open access by TopSCHOLAR®. It has been accepted for inclusion in Masters Theses & Specialist Projects by an authorized administrator of TopSCHOLAR®. For more information, please contact [topscholar@wku.edu](mailto:topscholar@wku.edu).

BIOMIMETIC STUDIES OF OXIDATION REACTIONS BY METALLOPORPHYRINS  
THROUGH LIGAND EFFECT AND KINETIC STUDIES OF PHOTO-GENERATED  
PORPHYRIN-IRON(IV)-OXO COMPOUND II MODELS

A Thesis  
Presented to  
The Faculty of the Department of Chemistry  
Western Kentucky University  
Bowling Green, Kentucky

In Partial Fulfillment  
of the Requirements for the Degree  
Master of Science

By  
Dharmesh J Patel

May 2018

BIOMIMETIC STUDIES OF OXIDATION REACTIONS BY METALLOPORPHYRINS  
THROUGH LIGAND EFFECT AND KINETIC STUDIES OF PHOTO-GENERATED  
PORPHYRIN-IRON(IV)-OXO COMPOUND II MODELS

Date Recommended 04-06-2018



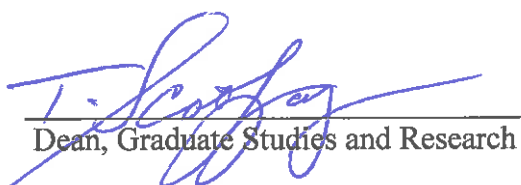
Dr. Rui Zhang, Director of Thesis



Dr. Darwin Dahl



Dr. Edwin Stevens



Dean, Graduate Studies and Research

4/19/18  
Date

## ACKNOWLEDGEMENTS

I would like to thank my advisor, Dr. Rui Zhang for his enormous support during my two-year master's program. It has been an honor and privilege to be able to conduct research under his guidance. I appreciate all his contributions of knowledge, time, ideas, and funding that made my MSc experience productive and stimulating. Believe it or not, he has taught me how good experimental chemistry is carried out, along with data collection and interpretation. The joy and enthusiasm he has for research is contagious and motivates me during hard times, especially when I am in the lab the whole day and unable to figure out why my experiment is not working or not getting the expected results. His open-door policy allows me to stop by anytime to clear doubts that I may have while conducting research. He is very understanding and has never stopped me from going to my mandatory training or attending family functions. No matter where I may be in the future, I will always remember that I had an excellent research guide in the form of a teacher and advisor, Dr. Rui Zhang.

The members of Dr. Zhang's research group have contributed immensely to my personal and professional time here at WKU. Our group has been a source of friendships as well as good advice and collaborations. I am especially grateful for the fun of the group members who stuck it out in grad school with me: Ka Wai Kwong, Ngo Fung Lee, Haiyan Liu, Haleh Jeddi, Jonathan Malone, Mike Winchester, Davis Ranburger, Benjamin Kash, and Dana Biechele-Speziale. I would like to acknowledge honorary group member Ka Wai Kwong, who was a former group leader. We worked together on the porphyrin experiment at the very beginning, and I very much appreciate his enthusiasm, integrity, and willingness to teach me in the research laboratory. The NMR

analysis studies discussed in this dissertation would not have been possible without the tremendous support from Dr. Lester Pesterfield, Dr. Kevin Williams, and Ms. Alicia Pesterfield. I would also like to thank the two other members on my thesis committee, Dr. Darwin Dahl, and Dr. Edwin Stevens, for their time and insightful guidance and questions. I want to thank Ms. Alicia Pesterfield for chemical supply, that is getting the chemical needed to research to me on a timely manner. For the chemistry department, I would like to thank Ms. Haley Smith, for answering all my questions and reminding me on deadlines for form submissions.

I gratefully acknowledge the funding sources that made my research work possible. My work was funded by the National Science Foundation and Kentucky EPSCoR program. I would like to give my sincere thanks to WKU Chemistry Department for their generous support. My stay at WKU was made enjoyable in large part due to many friends that became part of my life. I am grateful to Haiyan Liu, Amy Hoffman, Dewaker Dhandhapani, Sarah and Wouter Van-Alebeek, Toni Dye, among many others for their friendship and wonderful time we spent together.

Lastly, I would like to thank my wife, family, and relatives for all their love, encouragement and support during my stay at WKU considering the fact that they are 8100 miles away from me. If it were not for their support, I don't think I would have made it thus far and be able to go on for further studies.

Dharmesh J. Patel

May 2018

## TABLE OF CONTENTS

CHAPTER 1 .....	1
INTRODUCTION .....	1
1.1    General Overview of Cytochrome P450 Enzymes.....	1
1.2    Biomimetic Oxidations by Metalloporphyrins .....	6
1.3    Compound I and Compound II Species.....	9
1.4    Photochemical Generation of High-Valent Metal-Oxo Species .....	11
CHAPTER 2 .....	15
EXPERIMENTAL SECTION .....	15
2.1    Materials .....	15
2.2    Methods .....	16
2.2.1    Physical Measurements .....	16
2.2.2    General Photolysis Procedure of Iron(III) Porphyrin Bromates [Fe <sup>III</sup> (Por)(BrO <sub>3</sub> )] ...	17
2.2.3    Direct Kinetic Studies of High-Valent Metal-Oxo Intermediates .....	17
2.3    Synthesis and Characterization .....	19
2.3.1    Synthesis of 5,10,15,20-tetrakis(2,6-Difluorophenyl)porphyrin, H <sub>2</sub> (TDFPP) (1b) ...	19
2.3.2    Synthesis of Iron(III) Porphyrin Chloride [Fe <sup>III</sup> (Por)Cl] (2b) .....	21

CHAPTER 3 .....	24
PHOTOCHEMICAL GENERATION AND KINETIC STUDIES OF HIGH-VALENT PORPHYRIN-IRON(IV)-OXO COMPOUND II MODELS .....	24
3.1    Introduction .....	24
3.2    Results and Discussion.....	26
3.2.1    Synthesis of Iron(III) Porphyrin Bromate Precursors .....	26
3.2.2    Photo-Generation of High-Valent Iron(IV)-Oxo Porphyrins (Compound II Models)	27
3.2.4    Kinetic Studies of Oxidations by Photo-Generated Compound II Species .....	32
3.2.5    Mechanistic Consideration of Photo-generation of Compound II .....	39
CHAPTER 4 .....	44
CONCLUSION.....	44
REFERENCES .....	46
CURRICULUM VITAE.....	57
ABBREVIATIONS AND SYMBOLS.....	60

## LIST OF FIGURES

<b>Figure 1-1:</b> Iron(III) protoporphyrin IX linked with a proximal cysteine ligand.....	3
<b>Figure 1-2:</b> X-ray structure of cytochrome P450 <sub>cam</sub> .....	5
<b>Figure 2-1:</b> (A) Agilent 8454 diode array UV-visible spectrophotometer. (B) Agilent GC-MS system.....	17
<b>Figure 2-2.</b> (A) The UV-vis spectrum of [H <sub>2</sub> (TDFPP)] ( <b>1b</b> ) in CH <sub>2</sub> Cl <sub>2</sub> ; (B) The <sup>1</sup> H-NMR spectrum of [H <sub>2</sub> (TDFPP)] ( <b>1b</b> ) in CDCl <sub>3</sub> .....	20
<b>Figure 2-3.</b> (A) The UV-vis spectrum of [Fe <sup>III</sup> (TPFPP)Cl] ( <b>2a</b> ) in CH <sub>2</sub> Cl <sub>2</sub> ; (B) The <sup>1</sup> H-NMR spectrum of [Fe <sup>III</sup> (TPFPP)Cl] ( <b>2a</b> ) in CDCl <sub>3</sub> .....	22
<b>Figure 2-4.</b> (A) The UV-vis spectrum of [Fe <sup>III</sup> (TDFPP)Cl] ( <b>2b</b> ) in CH <sub>2</sub> Cl <sub>2</sub> ; (B) The <sup>1</sup> H-NMR spectrum of [Fe <sup>III</sup> (TDFPP)Cl] ( <b>2b</b> ) in CDCl <sub>3</sub> .....	23
<b>Figure 3-1.</b> (A) UV-vis spectra of [Fe <sup>IV</sup> (TPFPP)Cl] (dashed line) and [Fe <sup>III</sup> (TPFPP)(BrO <sub>3</sub> )] (solid line); (B) UV-vis spectra of [Fe <sup>IV</sup> (TPFPP)Cl] (dashed line) and [Fe <sup>III</sup> (TPFPP)(BrO <sub>3</sub> )] (solid line); .....	27
<b>Figure 3-2.</b> (A) Time-resolved spectra of <b>4b</b> following the irradiation of <b>3b</b> with visible light (120 W) in anaerobic CH <sub>3</sub> CN solution at 23 ± 2 °C over 20-30 min. (B) Time-resolved spectra of <b>4b</b> following chemical oxidation of <b>2b</b> with PhI(OAc) <sub>2</sub> (5 equiv.) over 5 min.....	28



<b>Figure 3-3.</b> (A) Time-resolved spectra of <b>4a</b> reacting in CH <sub>3</sub> CN with ethylbenzene (0.31 M) over 140 s. (B) Time-resolved spectra of <b>4b</b> reacting in CH <sub>3</sub> CN with ethylbenzene (0.24 M) over 140 s.....	34
<b>Figure 3-4.</b> Kinetic plots of the observed rate constants for the reactions of <b>4a</b> (A) and <b>4b</b> (B) versus the concentrations of ethylbenzene.....	35
<b>Figure 3-5.</b> (A) Time-resolved spectra of <b>4b</b> reacting in CH <sub>3</sub> CN with thioanisole (0.6 mM) over 60 s. (B) Kinetic plot of the observed rate constants for the reaction of <b>4b</b> versus the concentrations of thioanisole.....	35
<b>Figure 3-6.</b> (A) Plots of the observed pseudo-first-order rate constants versus different concentrations of thioanisole with <b>4a</b> . (B) Linear free-energy relationship for rate constants for reactions of <b>4a</b> with thioanisoles with $\sigma^+$ values.....	38
<b>Figure 3-7.</b> Observed apparent pseudo-first-order rate constants for reaction of <b>4b</b> in CH <sub>3</sub> CN in the presence of 4.0 mM thioanisole. The concentrations of precursor <b>3b</b> are listed under the photochemical conditions used in this study; the conversion of <b>3b</b> to <b>4b</b> was > 95%.....	42

## LIST OF SCHEMES

<b>Scheme 1-1:</b> Monooxygenase reaction.....	2
<b>Scheme 1-2:</b> Oxidations catalyzed by CYP450 enzymes.....	4
<b>Scheme 1-3:</b> Stereospecific hydroxylation of C-H bond at position 5 of the camphor catalyzed by CYP450 <sub>cam</sub> .....	6
<b>Scheme 1-4:</b> Typical metalloporphyrin-mediated reactions.....	7
<b>Scheme 1-5:</b> Chemical generation of compound I and compound II species.....	11
<b>Scheme 1-6:</b> Photo-induced ligand cleavage reactions for generation of high-valent transition metal-oxo species.....	13
<b>Scheme 2-1:</b> Two-step synthesis of [H <sub>2</sub> (Por)] ( <b>1a-b</b> ).....	19
<b>Scheme 2-2:</b> Synthesis of [Fe <sup>III</sup> (Por)Cl] ( <b>2a</b> and <b>2b</b> ).....	21
<b>Scheme 3-1:</b> Axial ligand exchange from <b>2a-b</b> to <b>3a-b</b> with Ag(BrO <sub>3</sub> ).....	26
<b>Scheme 3-2:</b> Photochemical generation of iron(IV)-oxo compound II models.....	28
<b>Scheme 3-3:</b> Mechanistic considerations on photochemical formation of iron(IV)-oxo neutral porphyrin (compound II) and iron(IV)-oxo porphyrin radical cations (compound I) by porphyrin ligands.....	30
<b>Scheme 3-4:</b> A disproportionation pathway for reactions of species <b>4</b> .....	40

## LIST OF TABLES

<b>Table 3-1.</b> Second-order rate constants ( $k_{ox}$ ) for reactions of porphyrin-iron-oxo species	
<b>4</b> .....	<b>36</b>

BIOMIMETIC STUDIES OF OXIDATION REACTIONS BY  
METALLOPORPHYRINS THROUGH LIGAND EFFECT AND KINETIC STUDIES  
OF PHOTO-GENERATED PORPHYRIN-IRON(IV)-OXO COMPOUND II MODELS

Dharmesh Patel

May 2018

Pages 61

Directed by: Rui Zhang, Darwin Dahl, and Edwin Stevens

Department of Chemistry

Western Kentucky University

High-valent iron(IV)-oxo porphyrins are the central oxidizing species in heme-containing enzymes and synthetic oxidation catalysts. Many transition metal complexes have been extensively studied as models of the ubiquitous cytochrome P450 enzymes to probe the sophisticated oxygen atom transfer (OAT) mechanism as well as to invent enzyme-like oxidation catalysts. In this work, two metalloporphyrin complexes have been successfully synthesized, and spectroscopically characterized. A new photochemical entry to porphyrin-iron(IV)-oxo derivatives, commonly referred to as compound II models, was also investigated in two porphyrin ligands that differ in electronic and steric environments. As determined by their distinct UV-vis spectra and kinetic behaviors, iron(IV)-oxo porphyrins  $[\text{Fe}^{\text{IV}}(\text{Por})\text{O}]$  were successfully produced by visible light irradiation of highly photo-labile porphyrin-iron(III) bromates. The iron(IV)-oxo porphyrins investigated in this study include 5,10,15,20-tetra(pentafluorophenyl)porphyrin-iron(IV)-oxo (**4a**), and 5,10,15,20-tetra(2,6-difluorophenyl)porphyrin-iron(IV)-oxo (**4b**).

As observed in both systems, the photochemical reactions may undergo a heterolytic cleavage of the O-Br bond in the ligands to form a putative iron(V)-oxo intermediate which undergoes a rapid comproportionation reaction with residual iron(III) to give the compound II species. The kinetics of OAT reactions with a variety of organic substrates performed by these photo-generated  $[\text{Fe}^{\text{IV}}(\text{Por})\text{O}]$  compounds were studied in  $\text{CH}_3\text{CN}$  solutions. Apparent second-order rate constants determined under pseudo-first-order conditions for sulfide oxidation reactions are  $(2.0 \pm 0.2) \times 10^2 - (2.6 \pm 0.5) \times 10^1 \text{ M}^{-1}\text{s}^{-1}$ , which are 3 to 4 orders of magnitude greater in comparison to those of alkene epoxidations and activated C-H bond oxidations by the same oxo species. Conventional Hammett analyses gave a non-linear correlation, indicating no significant charge developed at the sulfur during the oxidation process. For a given substrate, the reactivity order for the iron(IV)-oxo species was **4a** < **4b**, which is inverted with respect to expectation based on the electron-withdrawing properties of the porphyrin macrocycles. The absolute rate constants from the kinetic studies provided insight into the transient oxidants in catalytic reactions under turnover conditions where actual reactive oxidants are not observable. The kinetic results strongly suggest that neutral iron(IV)-oxo porphyrin (**4**) may undergo a disproportionation reaction to form higher oxidized iron(IV)-oxo porphyrin radical cations as the true oxidant.

# CHAPTER 1

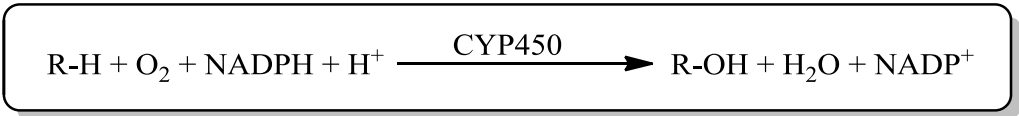
## INTRODUCTION

### 1.1 General Overview of Cytochrome P450 Enzymes

In synthetic organic chemistry, catalytic oxidation of organic substrate is known to be of great importance for the production of chemicals and pharmaceuticals. Catalytic oxidation is also the key to understanding fundamental transformations in Nature.<sup>1</sup> So far many chemicals, such as alcohols, carbonyl compounds, and epoxides have been produced by catalytic oxidations. However, most of the oxidations were performed with stoichiometric amounts of undesirable solvents that generate large amounts of toxic waste.<sup>2</sup> Therefore with an increasing environmental concern, the development of new processes employing transition metals as substrate-selective catalysts with utilization of mild and clean environmentally friendly oxidants for selective oxidations are becoming one of the most significant goals in oxidation chemistry.<sup>2d, 3</sup> Particularly, molecular oxygen and hydrogen peroxide are atom efficient and produce water as the only by-product, hence becoming more important in chemical manufacturing.<sup>2c</sup>

In biological systems, catalytic oxidations facilitated by oxidation enzymes are fundamental in many biosynthesis and biodegradation processes.<sup>4</sup> Most of the biological oxidations are mediated by heme-containing oxygenases notably the ubiquitous cytochrome P450 monooxygenase (CYP450), and transition metal catalysts have been synthesized to mimic the metalloenzymes in Nature. CYP450s were discovered over six decades ago by Axelrod and Brodie, et al., who identified an enzyme system in the endoplasmic reticulum of the liver which was able to oxidize xenobiotic compounds.<sup>5</sup>

These monooxygenases are a ubiquitous family of metabolizing heme-proteins that play a key role in oxidative transformations of endogenous and/or exogenous molecules, and have been found in a wide range of life species including plants, fungi, bacteria, insects, and mammals.<sup>6</sup> The CYP450 enzymes activate molecular oxygen, inserts one oxygen atom into a substrate, and reduces the second oxygen to a water molecule utilizing two electrons from reducing agents such as NADH or NADPH via a reductase protein (Scheme 1-1).<sup>7</sup> The CYP450 enzymes are termed as monooxygenases because only one of the two oxygen atoms from the molecular oxygen is incorporated into the organic substrate.



**Scheme 1-1:** Monooxygenase reaction.

In 1958, Klingenberg and Garfinkel established that the rat liver microsomes contained an unknown carbon monoxide binding pigment which has an absorption at 450 nm.<sup>8</sup> This was later demonstrated to be a b-type class heme-protein having a strong absorption peak at 450 nm, therefore the pigment was named as CYP450.<sup>9</sup> CYP450 is a heme-thiolate enzyme that catalyzes many biological oxidation processes,<sup>10</sup> including many biosynthesis and biodegradation processes.<sup>4</sup> Since its discovery, 60 CYP450 genes and 58 pseudogenes have been isolated from numerous mammalian tissues such as liver, kidney, lungs, and intestine.<sup>7</sup> The most common heme prosthetic group (active site) found in heme-containing enzymes is the iron protoporphyrin IX complex, covalently

linked to protein by the sulfur atom of a proximal cysteine ligand, and reported to leave a coordination site open to bind and activate molecular oxygen (Figure 1-1).<sup>4,7</sup>

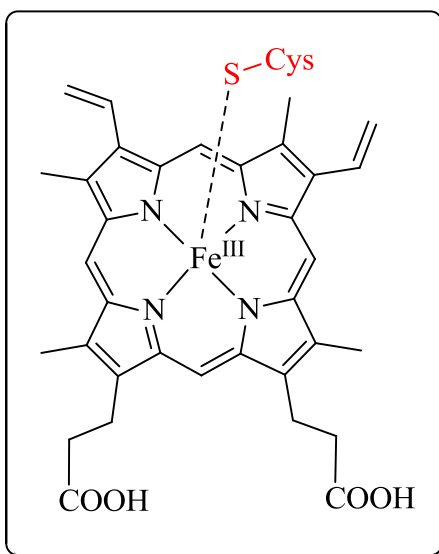
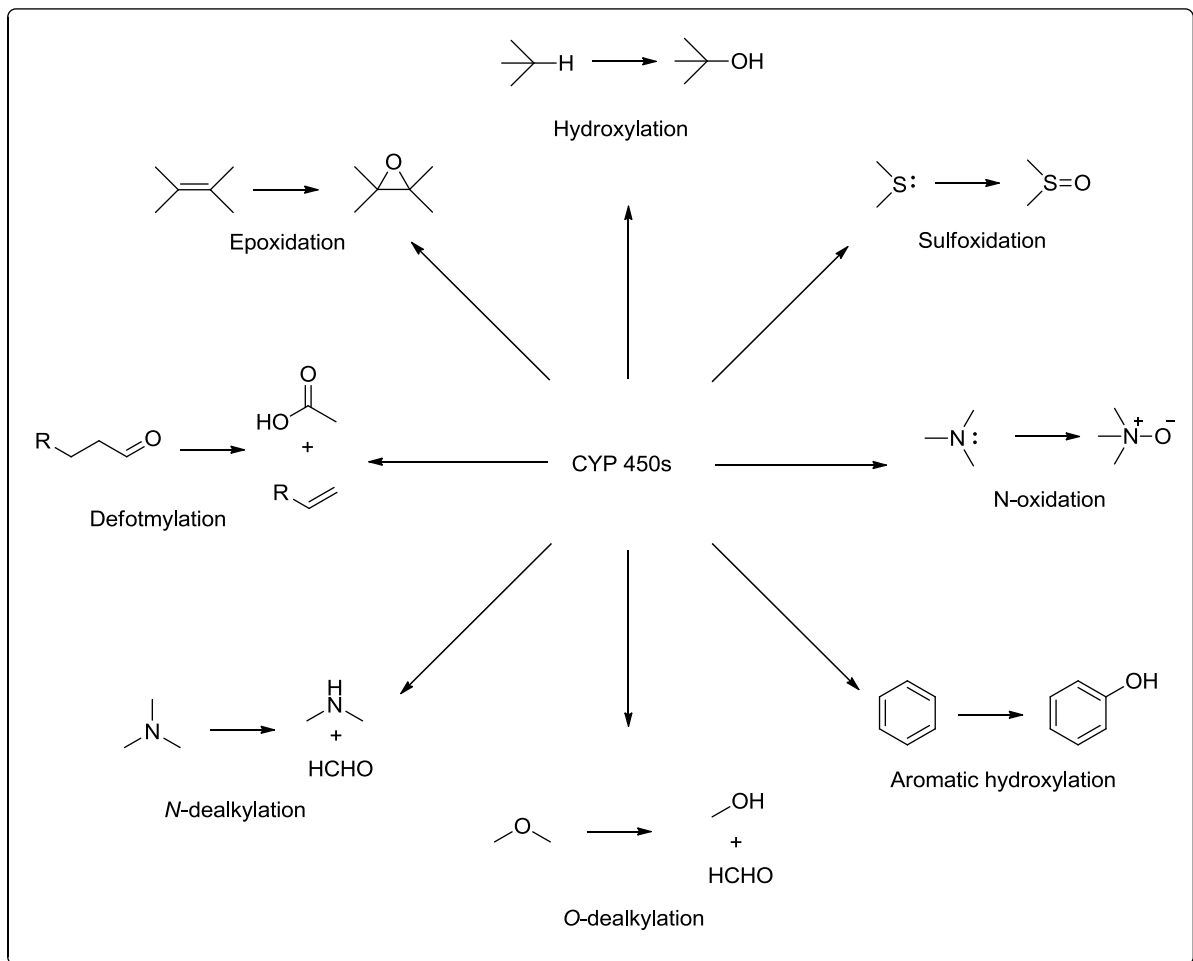


**Figure 1-1.** Iron(III) protoporphyrin IX linked with a proximal cysteine ligand.

The CYP450 enzymes are one of the most studied metalloenzymes due to their significant role in the metabolism of xenobiotics as a protective role of degradation for excretion and in catalyzing biosynthesis of critical signaling molecules for control of development and homeostasis.<sup>11</sup> The CYP450 enzymes have unique ability to accomplish a wide variety of difficult enzymatic steps, which include substrate binding, electron transfer, oxygen binding and substrate oxidation, many of which are characterized by high degrees of chemo-, regio, and enantioselectivities (Scheme 1-2).<sup>7, 12</sup> In 1970, CYP450s involvement in steroid biosynthesis along with its central function in drug metabolism led to its extensive investigation in biochemical systems.<sup>1b, 13</sup>





**Scheme 1-2:** Oxidations catalyzed by CYP450 enzymes.

Primarily, CYP450s have been classified as electron-transfer proteins that provide electrons from NADH or NADPH to the oxygenase protein.<sup>14</sup> CYP450s are also classified into two Classes in drug metabolism, i.e., Class I corresponds to mammalian mitochondrial enzymes involved in steroid synthesis and Class II corresponds to mammalian enzymes located in the endoplasmic reticulum of liver cells.<sup>15</sup> A specific group of isoforms are expressed in the liver with the role of metabolizing xenobiotic compounds, particularly six of these CYP450 isoforms are important in drug metabolism as they comprise approximately 90% of the metabolism of pharmaceutical drugs.<sup>16</sup> The

interactions with warfarin, antidepressants, antiepileptic drugs, and statins often involve the CYP450s. Since then, the study of CYP450s have focused on minimizing the possibility of adversative drug reactions and interactions.<sup>17</sup>

The structurally and biochemically best-characterized CYP450 is a soluble bacterial monooxygenase (CYP450<sub>cam</sub>) discovered in *Pseudomonas putida* by Poulos and co-workers in 1985.<sup>18</sup> The enigma of the cytochrome P450s was deciphered when Poulos, et al., provided the first three-dimensional structure in 1986 (Figure 1-2).<sup>19</sup>

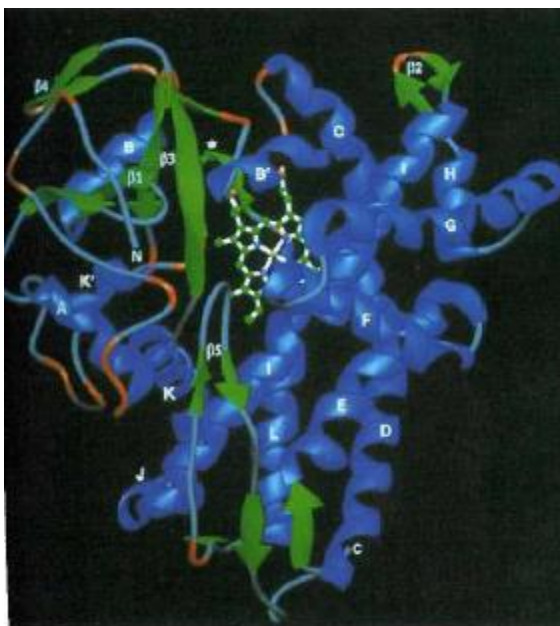
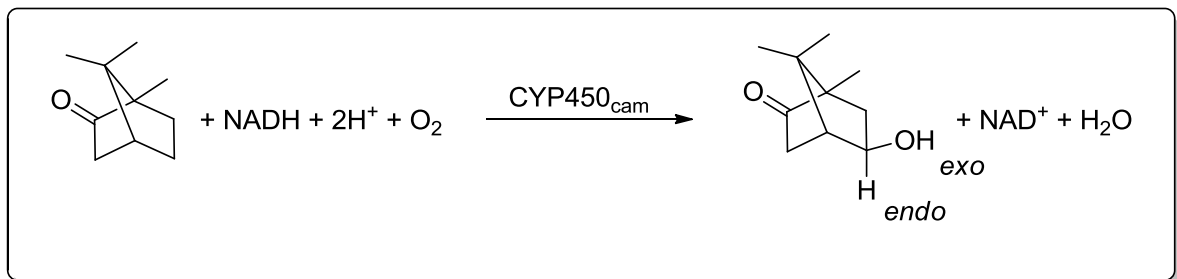


**Figure 1-2:** X-ray structure of cytochrome P450<sub>cam</sub>.

CYP450<sub>cam</sub> of *Pseudomonas putida* catalyzes the regio- and stereospecific hydroxylation of the bicyclic camphor molecule with molecular oxygen to form 5-*exo*-hydroxycamphor (Scheme 1-3).<sup>8a</sup>



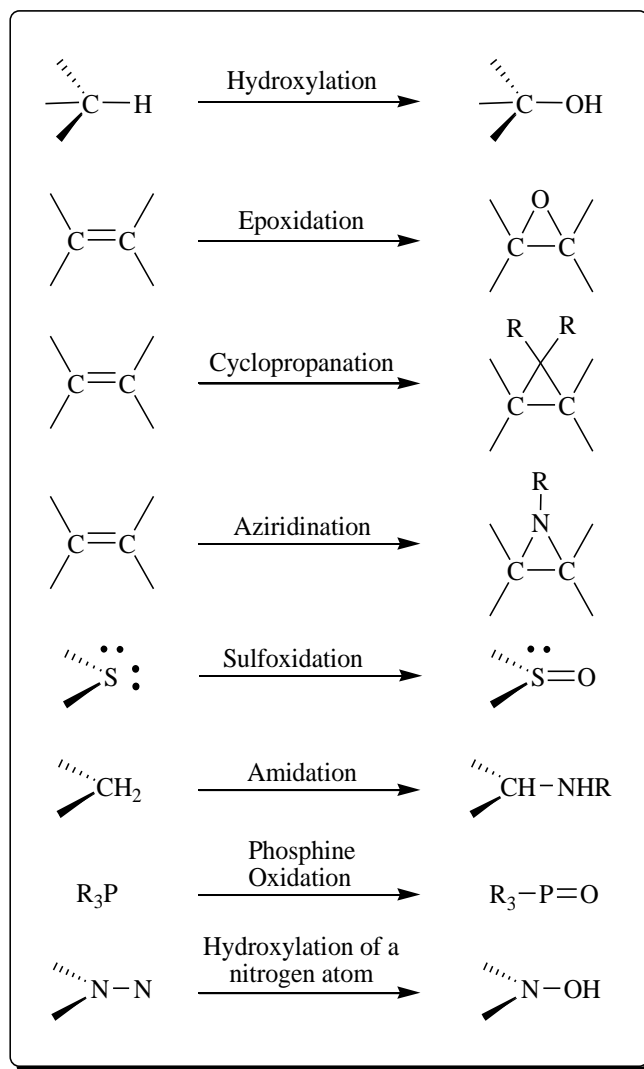
**Scheme 1-3.** Stereospecific hydroxylation of the C-H bond at position 5 of camphor catalyzed by CYP450<sub>cam</sub>.

Numerous metalloporphyrin complexes have been synthesized as models of CYP450 enzymes and biomimetic catalysts for selective oxidations, solely because of the instability and difficulty in the purification of the CYP450s.<sup>20</sup> This interest was stimulated by a desire for better understanding of the intricate mechanisms of the biochemical pathways and the expectation that relatively simple model systems could emulate the selective oxidations of hydrocarbons catalyzed by CYP450 enzymes.

## 1.2 Biomimetic Oxidations by Metalloporphyrins

Effective catalytic systems for hydrocarbon oxidations based on metalloporphyrin catalysts with iron, manganese, and ruthenium porphyrins have received considerable attention for decades.<sup>2d</sup> Numerous cytochrome P450 models have been developed and applied to hydrocarbon oxidations with the aim of both developing useful catalysts and probing the mechanisms of the processes.<sup>21</sup> Most biological oxidations mediated by CYP450 enzymes are highly, often completely, stereo-selective and ecologically sustainable. Metalloporphyrins have been widely used as biomimetic models of cytochrome P450 enzymes to catalyze a variety of oxidation reactions (Scheme 1-4). The first metalloporphyrin oxidation system reported was iron porphyrin in 1979, with

iodosylbenzene as the oxygen source and  $\text{Fe}^{\text{III}}(\text{TPP})\text{Cl}$  (TPP = *meso*-tetraphenylporphyrin) as the catalyst that catalyzed effective stereospecific alkene epoxidation and alkane hydroxylation reactions.<sup>1a, 22</sup>



**Scheme 1-4.** Typical metalloporphyrin-mediated reactions.

Most often in biomimetic catalytic oxidation, a transition metal catalyst is oxidized to a high-valent metal-oxo species by a sacrificial oxidant, then the activated transition metal-oxo intermediate oxidizes the substrate.<sup>8a, 21</sup> Many transition metal

catalysts, with a core structure closely resembling that of the iron porphyrin core of CYP450 enzymes, have been synthesized as models to produce enzyme-like oxidation catalysts as well as to probe the sophisticated mechanism of molecular oxygen activation.<sup>1a</sup> Among the most extensively studied systems are the epoxidation of alkenes and hydroxylation of alkenes catalyzed by transition metals in macrocyclic porphyrin ligands.<sup>23</sup>

Studies using the synthetic metalloporphyrins as biomimetic models of cytochrome P450s have presented scientists with important tools useful to probe the nature of the enzymatic process.<sup>21, 24</sup> The sacrificial oxidants compatible with metalloporphyrins were mostly restricted to PhIO, NaOCl, H<sub>2</sub>O<sub>2</sub>, <sup>t</sup>BuOOH (*tert*-butylhydroperoxide), KHSO<sub>5</sub> and oxaziridines.<sup>21</sup> However, molecular oxygen can be also used in the presence of an electron source.<sup>25</sup> The use of H<sub>2</sub>O<sub>2</sub> often results in oxidative degradation of the catalyst due to the potency of this oxidant.<sup>26</sup> Synthetic manganese porphyrin complexes have shown catalytic promise as CYP450 enzyme models in oxidation reaction in the past decades.<sup>21, 27</sup>

High-valent transition metal-oxo transients with high reactivity have been invoked as the active oxidizing species in many metal-catalyzed oxidations.<sup>8a</sup> However, in most catalytic reactions, the concentration of active metal-oxo oxidants do not build up to detectable amounts. For example, highly reactive porphyrin-manganese(V)-oxo derivatives were proposed as the key intermediates in catalytic processes for decades, but they eluded detection until the year 1997 when Groves and co-workers reported the first manganese(V)-oxo porphyrin complex.<sup>28</sup> Ruthenium porphyrin complexes have been developed as enzyme-like catalysts for selective oxidation methods due to its close

periodic relationship to iron.<sup>11b</sup> In addition, high-valent ruthenium-oxo porphyrin intermediates have been extensively studied as OAT agents, which exhibit significant reactivity towards organic substrates such as alcohols and hydrocarbons.<sup>2d, 29</sup>

### 1.3 Compound I and Compound II Species

In enzymatic and synthetic oxidations, high-valent iron-oxo species have been identified as the key oxidizing intermediates in the catalytic cycles of oxygen activating iron enzymes, as well as synthetic biomimetic catalysts.<sup>7-8, 30</sup> Hence, iron-oxo complexes have received significant attention because of their synthetic utility in various oxidation reactions and relevance to a variety of oxidative enzymes in nature.<sup>7, 30b, 31</sup> In heme-containing enzymes, an iron(IV)-oxo porphyrin radical cation species, biologically termed as Compound I, has been characterized in the catalytic cycles of peroxidase and catalase enzymes.<sup>32</sup> In general, these heme-containing enzymes consist of the same iron protoporphyrin IX complex, but different heme-proximal ligands.<sup>33</sup> Compound I transients are also thought to be the oxidizing transient in the cytochrome P450 enzymes.<sup>12</sup> The recent advanced spectroscopic characterization and kinetic studies suggest that compound I transients are involved in cytochrome P450 enzymes.<sup>34</sup>

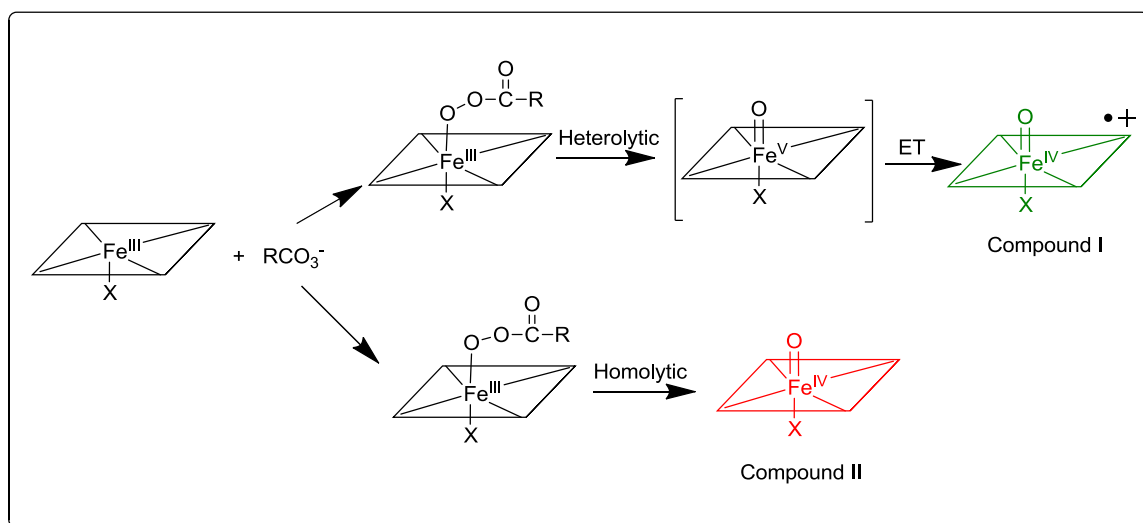
Non-heme iron(V)-oxo intermediates have been reported to be the reactive intermediates in the Rieske dioxygenase enzymes and their synthetic functional models.<sup>35</sup> True iron(V)-oxo complexes are usually rare and elusive, and are considered to be more reactive than the iron(IV)-oxo ligand radical cations, compound I species.<sup>36</sup> For example, Collins *et al.* reported an iron(V)-oxo complex supported by a tetraanionic ligand that displayed truly unprecedented reactivity.<sup>35</sup> The putative porphyrin-iron(V)-oxo transients

produced by laser flash photolysis (LFP) methods displayed an appropriate high level of reactivity.<sup>37</sup>

The fast mixing studies of CYP450s with an external oxidant produced transient compound I species within milliseconds by the freeze-quench technique.<sup>38</sup> Therefore, synthetic iron porphyrin complexes have been widely used as models of heme-containing enzymes with the sole purpose of gaining an understanding of the enzymatic reaction mechanism. Numerous studies have shown that compound I species were formed from the reactions of iron(III) porphyrin complexes and various oxidants, such as *m*-chloroperoxybenzoic acid, iodosobenzene, and ozone.<sup>37, 39</sup> In 1981 Groves and co-workers reported the first preparative generation and characterization of a compound I like model species.<sup>40</sup> The oxidation of iron-porphyrin chloride complex [Fe<sup>III</sup>(TMP)Cl] (TMP = 5,10,15,20-tetramesitylporphyrin) with 1.5 equivalents of *m*CPBA at -78 °C generated an iron(IV)-oxo porphyrin radical cation species (Compound I).

On the other hand, the one-electron reduced form of porphyrin-iron(IV)-oxo intermediates, commonly called compound II, act as reactive species<sup>30a, 41</sup> particularly in one electron-transfer oxidations reactions such as C-H activation and hydride-transfer reactions.<sup>42</sup> The preparation and characterization of the iron(IV)-oxo neutral porphyrins compound II have been known for nearly two decades now.<sup>43</sup> Iron(IV)-oxo neutral porphyrin are generally more stable, hence, less reactive in OAT reactions as comparison to compound I species.<sup>44</sup> Groves and co-workers also reported the oxidation reaction with 1 equiv. of PhIO at -78 °C in CH<sub>2</sub>Cl<sub>2</sub> gave an iron(IV)-oxo compound II species.<sup>40</sup>

Typically the iron(V)-oxo species would be generated directly from the heterolytic peroxy bond cleavage after the second protonation on the distal O-H atom. Depending on the energy barrier for internal electron transfer (ET), the first-formed iron(V)-oxo transient could serve as either an intermediate or a transition state in the oxidation process (Scheme 1-5).<sup>41a</sup>



**Scheme 1-5.** Chemical generation of compound I and compound II species.

Our research group has recently discovered a photochemical approach to access compound I and compound II species.<sup>45</sup> Controlled by the electronic nature of porphyrin ligands, iron(IV)-oxo porphyrin radical cations (compound I models) and iron(IV)-oxo porphyrin derivatives (compound II models) were produced, by visible light irradiation of the corresponding iron(III) bromate complexes.

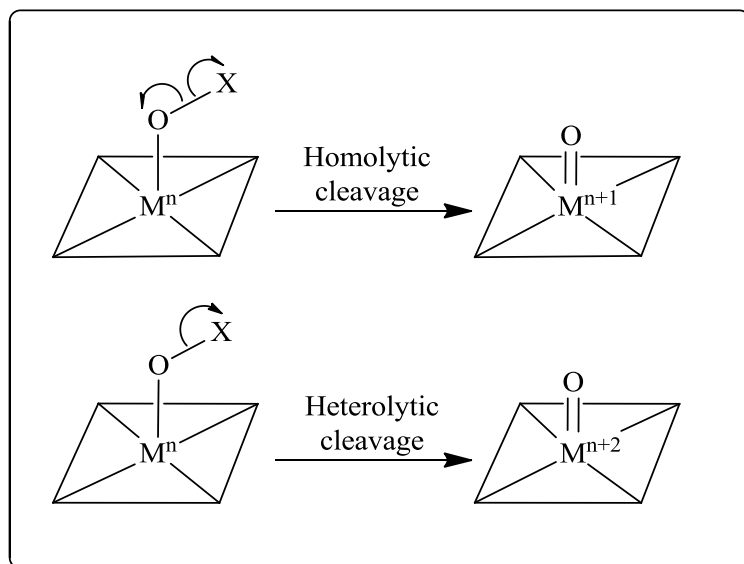
#### 1.4 Photochemical Generation of High-Valent Metal-Oxo Species

In metal-oxo chemistry, the photochemical reactions are intriguing and intrinsically advantageous because the activation is obtained through absorption of a



photon, hence leaving no residue.<sup>46</sup> In contrast, most chemical methods involved use of toxic or polluting reagents that are not environmentally friendly. Therefore, using visible light to induce reversible redox processes of the metal center could avoid all the disadvantages deriving from the use of chemical reagents.<sup>3b</sup> Notable, photochemical activation of transition metal complexes to produce reactive oxidants has been known for decades.<sup>47</sup> The photochemical approach produces metal-oxo species essentially instantly, permitting direct detection and allowing access to time scales that are much shorter than the fastest mixing experiments.

More importantly, the kinetics of oxidation reactions by photo-generated metal-oxo species are not convoluted with the rate constants for formation of the reactive transients by reaction of the excess sacrificial oxidant with the low-valent metal species.<sup>48</sup> Newcomb and co-worker have developed a photo-induced ligand cleavage reactions for production of high-valent transition metal-oxo derivatives.<sup>37, 39a, 49</sup> Notably, the use of laser flash photolysis methods to generate a variety of high-valent transition metal-oxo species supported by porphyrin and corrole ligands have been well developed.<sup>37, 39a, 49</sup> The concept of photo-induced ligand cleavage reaction is illustrated in Scheme 1-6. The precursor complexes have metal in the “n” oxidation state and an oxygen-containing ligand. Photolysis resulted in homolytic cleavage of the O-X bond in the ligand to give an “n + 1” oxidation state metal-oxo species; it may also proceed by heterolytic cleavage of the O-X bond in the ligand to give an “n + 2” oxidation state metal-oxo species.



**Scheme 1-6.** Photo-induced ligand cleavage reactions for generation of high-valent transition metal-oxo species.

The photochemical methods for formation of high-valent metal-oxo species require considerable development of requisite photochemical methods and especially photo-labile precursors. Photo-induced ligand cleavage reactions were used to produce *trans*-dioxoruthenium(VI) porphyrins, as well as a putative ruthenium(V)-oxo species.<sup>50</sup> This photochemical method can efficiently generate the high-valent metal-oxo complexes without the limitation of porphyrin ligands as observed in chemical methods.

Our recent kinetic and spectral studies also illustrated that the photo-generated manganese(V)-oxo corroles may oxidize the substrate through different oxidation pathways, depending on the nature of corrole ligand and the reaction medium.<sup>53</sup> Very recently, we communicated a visible light-induced formation of iron(IV)-oxo porphyrin radical cations (compound I models) and iron(IV)-oxo porphyrin (compound II models), which was controlled by the electronic nature of porphyrin ligands.<sup>45</sup> In this work, visible

light induced-ligand cleavage reactions have been extended for the generation and study of the high-valent iron(IV)-oxo intermediates supported by porphyrin ligands.

## CHAPTER 2

### EXPERIMENTAL SECTION

#### 2.1 Materials

All commercial reagents were of the best available purity and were used as supplied unless otherwise specified. All organic solvents used for synthesis and purification were purchased from Sigma-Aldrich Chemical Co., including acetone, acetonitrile, benzene, chloroform, cyclohexene, dichloromethane, ethanol, ethyl benzene, methanol, and *N,N*-dimethylformamide (DMF). HPLC grade acetonitrile (99.93%) was distilled over P<sub>2</sub>O<sub>5</sub> prior to use. All organic substrates for kinetic and catalytic oxidation studies were purified by passing through a flash chromatography column of active alumina (Grade 1) before use, including styrene, 4-fluorostyrene, 4-chlorostyrene, 4-methylstyrene, 4-vinylanisole, *cis*-stilbene, cyclohexene, *cis*-cyclooctene, diphenylmethane, diphenylmethanol, phenylethanol, ethylbenzene, ethylbenzene-*d*<sub>10</sub>, thioanisole, 4-fluorothioanisole, 4-chlorothioanisole, 4-methylthioanisole, 4-methoxythioanisole. The pyrrole for porphyrin synthesis was freshly distilled before use. 2,6-Difluorobenzaldehyde, 2,6-dichlorobenzaldehyde, hydrochloric acid (HCl), boron trifluoride diethyl etherate (BF<sub>3</sub>·OEt<sub>2</sub>), 2,3-dichloro-5,6-dicyano-*p*-benzequinone (DDQ), (diacetoxyiodo)benzene [PhI(OAc)<sub>2</sub>], *meta*-chloroperoxybenzoic acid (*m*-CPBA), 5,10,15,20-tetrakis(pentafluorophenyl)porphyrin, H<sub>2</sub>(TPFPP)(**1a**), iron(II) chloride, propanoic acid, and chloroform-*d* were obtained from Sigma-Aldrich Chemical Co. and used as such. All bromate or chlorate salts of metalloporphyrin complexes were prepared *in situ* by stirring excess amounts of silver bromate (AgBrO<sub>3</sub>) or silver chlorate (AgClO<sub>3</sub>) with [Fe<sup>III</sup>(Por)Cl]. 5,10,15,20-Tetrakis(2,6-difluorophenyl)porphyrin, abbreviated as

H<sub>2</sub>(TDFPP)(**1b**), was prepared according to known methods.<sup>51</sup> All iron(III) chloride complexes Fe<sup>III</sup>(Por)Cl (**2**, Por = **a-b**) used in this work were prepared by the literature reported method<sup>52</sup> and characterized by <sup>1</sup>H-NMR and UV-vis, matching the reported spectra.

## **2.2 Methods**

### **2.2.1 Physical Measurements**

<sup>1</sup>H-NMR was performed on a JEOL ECA-500 MHz spectrometer at 298K with tetramethylsilane (TMS) as internal standard. Chemical shifts (ppm) are reported relative to TMS. Visible light was produced from a SOLA SE II light engine (Lumencor) configured with a liquid light guide (6-120 W) or from a tungsten lamp (60-300 W). Kinetic measurements were performed with an Agilent 8453/4 diode array UV-vis spectrophotometer (Figure 2-1A). Gas chromatographic analysis was performed using an Agilent GC7820A/MS5975 with a flame ionization detector (FID) using a J&W Scientific Cyclodex-B capillary column (Figure 2-1B), coupled with an auto sample injector.

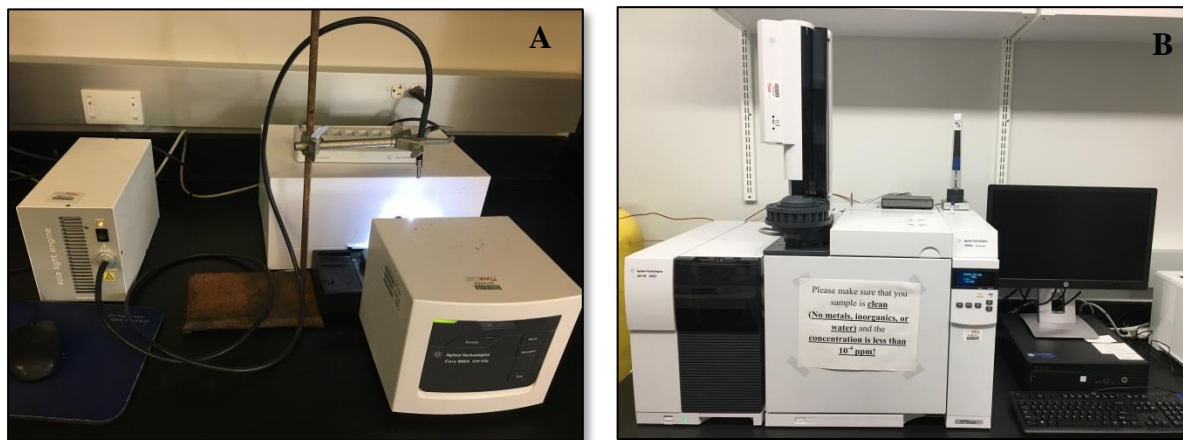


**Figure 2-1.** (A) Agilent 8454 diode array UV-visible spectrophotometer. (B) Agilent GC-MS system.

### 2.2.2 General Procedure for Photolysis of Iron(III) Porphyrin Bromates

#### [Fe<sup>III</sup>(Por)(BrO<sub>3</sub>)]

Facile exchange of the porphyrin complexes [Fe<sup>III</sup>(Por)Cl] (**2**) with excess amounts of Ag(BrO<sub>3</sub>) in anaerobic CH<sub>3</sub>CN (2 mL) gave the corresponding photo-labile bromate complexes [Fe<sup>III</sup>(Por)(BrO<sub>3</sub>)] (**3**) that were used for photochemical reactions. (**Caution!** Bromate salts of metal complexes are potentially explosive and should be handled with care.) The prepared solution of **3** with a concentration of  $1.0 \times 10^{-5}$  M was irradiated under visible light from a SOLA engine (120 W) at ambient temperature, and formation of the iron(IV)-oxo compound II species (**4**) was complete in a period of 5-20 min, as monitored by UV-vis spectroscopy.

### 2.2.3 Direct Kinetic Studies of High-Valent Metal-Oxo Intermediates

Reactions of high-valent metal-oxo compounds with excess amounts of organic substrates were conducted in 2 mL solutions at  $23 \pm 2$  °C. The rates of the reactions,

which represented the rates of oxo group transfer from high-valent iron(IV)-oxo (**4**) to substrate, were monitored by the decay of the Soret band of the high-valent metal-oxo species. Kinetics were measured under single-turnover conditions using a large excess of substrate to achieve pseudo-first-order kinetic conditions. Rate constants for reactions with substrates were determined from kinetic measurements with varied concentrations of substrate. The kinetic traces at  $\lambda_{\text{max}}$  of the Soret band displayed good pseudo-first-order behavior for at least four half-lives, and the data was solved to give pseudo-first-order observed rate constants,  $k_{\text{obs}}$ . The plots of these values against concentration of substrate were linear in all cases.

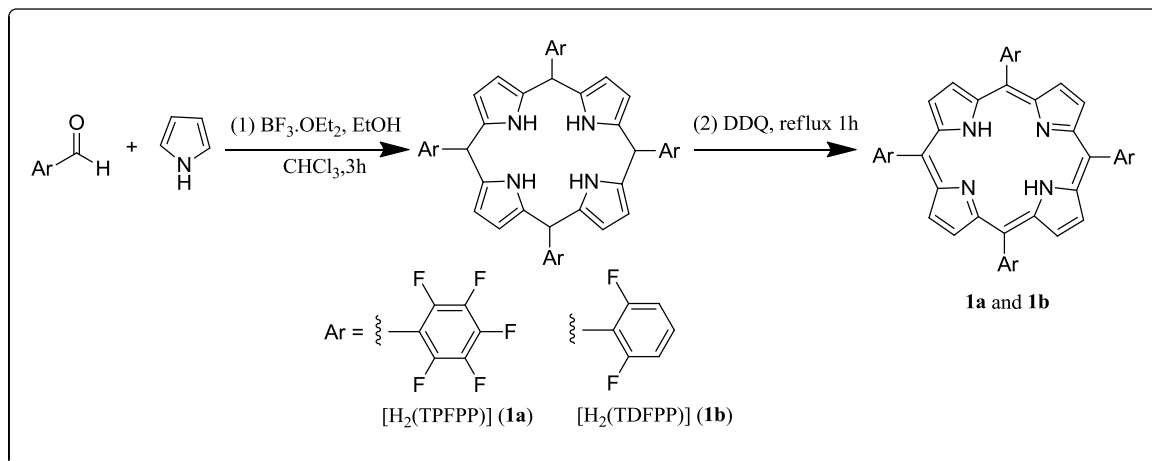
The second-order rate constants for reaction of the oxo species with the organic substrates were solved according to Eq. 1, where  $k_0$  is a background rate constant found in the absence of substrate,  $k_{\text{ox}}$  is the second-order rate constant for reaction with the substrate, and [Sub] is the concentration of substrate. All second-order rate constants are averages of 2-3 determinations consisting of independent kinetic measurements. Errors in the rate constants were reported at  $2\sigma$ .

$$k_{\text{obs}} = k_0 + k_{\text{ox}}[\text{Sub}] \quad (\text{Eq. 1})$$

## 2.3 Synthesis and Characterization

### 2.3.1 Synthesis of 5,10,15,20-tetrakis(2,6-Difluorophenyl)porphyrin, H<sub>2</sub>(TDFPP)

(1b)



**Scheme 2-1.** Two-step synthesis of [H<sub>2</sub>(Por)] (1a-b).

The sterically hindered porphyrin ligands (**1b**) were synthesized based on the well-known method.<sup>51</sup> To a 1L three-neck round-bottomed flask fitted with a septum, reflux condenser, and nitrogen inlet port was charged with 500 mL of chloroform, difluorobenzaldehyde (710  $\mu\text{L}$ , 5 mmol), pyrrole (350  $\mu\text{L}$ , 5 mmol) and ethyl alcohol (3.47 mL; 0.5% v/v) as a co-catalyst. The solution was then purged with argon for 5 min, followed by dropwise addition of boron trifluoride diethyl etherate ( $\text{BF}_3 \cdot \text{OEt}_2$ ) (660  $\mu\text{L}$ , 1.65 mmol). The solution changed from colorless to dark greenish brown gradually and was stirred at room temperature for 3 h. This reaction was monitored by UV-vis to confirm that porphyrinogen had been formed. At the end of 1st-step reaction, 2, 3-dichloro-5, 6-dicyano-*p*-benzequinone (DDQ) (966 mg) was added in powder form and the reaction mixture was gently refluxed for 1 h. The reaction mixture was then cooled to room temperature, and triethylamine (230  $\mu\text{L}$ , 1.65 mmol) was added to neutralize the



reaction mixture. The solution was evaporated to dryness. The dry solid crude product was scraped from the flask, placed on a filter, and washed with methanol until the filtrate was clear. After that, the product (**b**) was placed into a wet column (silica gel) and eluted with dichloromethane.

### 5, 10, 15, 20-tetrakis(2,6-Difluorophenyl)porphyrin [ $H_2$ (TDFPP)] (**1b**)

Yield = 184 mg (18.6%).

UV-vis ( $CH_2Cl_2$ )  $\lambda_{max}/nm$ : 413 (Soret), 507. (Figure 2-2A)

$^1H$ -NMR (500MHz,  $CDCl_3$ ):  $\delta$ , ppm: -2.78 (s, 2H, NH), 7.78 (m, 12H, *m*-ArH and *p* ArH), 8.87 (s, 8H,  $\beta$ -pyrrolic-H). (Figure 2-2B)

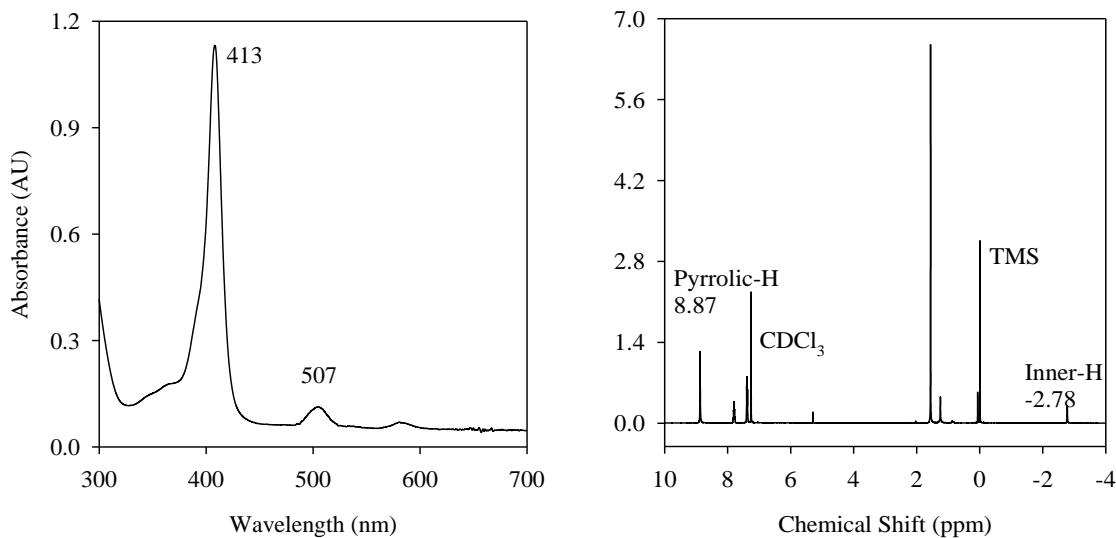
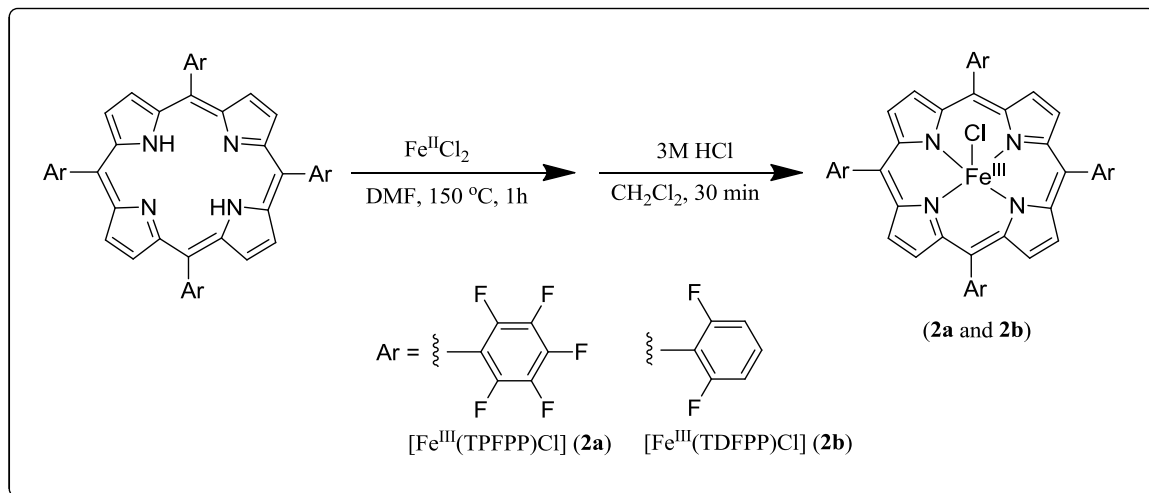


**Figure 2-2.** (A) The UV-vis spectrum of [ $H_2$ (TDFPP)] (**1b**) in  $CH_2Cl_2$ ; (B) The  $^1H$ -NMR spectrum of [ $H_2$ (TDFPP)] (**1b**) in  $CDCl_3$ .

### 2.3.2 Synthesis of Iron(III) Porphyrin Chloride [Fe<sup>III</sup>(Por)Cl] (**2b**)



**Scheme 2-2.** Synthesis of [Fe<sup>III</sup>(Por)Cl] (**2a** and **2b**).

The porphyrin free ligands employed in this study included [H<sub>2</sub>(TPFPP)] (**1a**), and [H<sub>2</sub>(TDFPP)] (**1b**). The iron(III) porphyrin complexes (**2**) were prepared as shown in Scheme 2-2.<sup>52</sup> In a typical procedure, to a 100 mL round-bottomed flask fitted to a reflux condenser, DMF (30 mL) was added and purged under argon for 5 min, then followed by addition of the porphyrin free ligand (**1**) (100 mg, 0.132 mmol) and iron(II) chloride (500 mg). The mixture was then refluxed for 1-2 h. This reaction was monitored by TLC analysis. The DMF solvent was then evaporated to dryness under vacuum, and the crude product was dissolved in dichloromethane. 3 M hydrochloric acid was added to the mixture, which was stirred for 15-30 min, to exchange the axial ligand from OAc to Cl. Extraction was performed with dichloromethane, then followed by deionized water. Na<sub>2</sub>SO<sub>4</sub> was added to remove any remaining traces of water. The product was then purified on a wet silica column using CH<sub>2</sub>Cl<sub>2</sub> as eluent.

**Iron(III) 5, 10, 15, 20-tetrakis(Pentafluorophenyl)porphyrin Chloride (2a)**

UV-vis ( $\text{CH}_2\text{Cl}_2$ )  $\lambda_{\text{max/nm}}$ : 407 (Soret), 352, 498, 562. (Figure 2-3A)

$^1\text{H-NMR}$  (500MHz,  $\text{CDCl}_3$ ):  $\delta$ , ppm: 82.6 (s, 8H,  $\beta$ -pyrrolic-H). (Figure 2-3B)

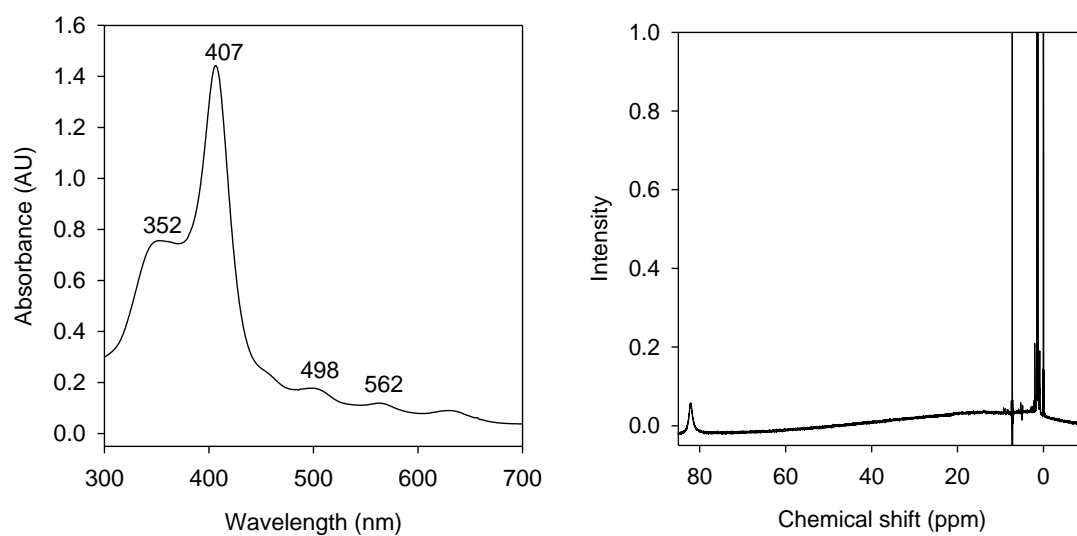


**Figure 2-3.** (A) The UV-vis spectrum of  $[\text{Fe}^{\text{III}}(\text{TPFPP})\text{Cl}]$  (**2a**) in  $\text{CH}_2\text{Cl}_2$ ; (B) The  $^1\text{H-NMR}$  spectrum of  $[\text{Fe}^{\text{III}}(\text{TPFPP})\text{Cl}]$  (**2a**) in  $\text{CDCl}_3$ .

**Iron(III) 5, 10, 15, 20-tetrakis(2,6-Difluorophenyl)porphyrin Chloride (2b)**

Yield = 82 mg (82 %).

UV-vis ( $\text{CH}_2\text{Cl}_2$ )  $\lambda_{\text{max/nm}}$ : 412 (Soret), 366, 505, 572. (Figure 2-3A)

$^1\text{H-NMR}$  (500MHz,  $\text{CDCl}_3$ ):  $\delta$ , ppm: 82.6 (s, 8H,  $\beta$ -pyrrolic-H). (Figure 2-3B)

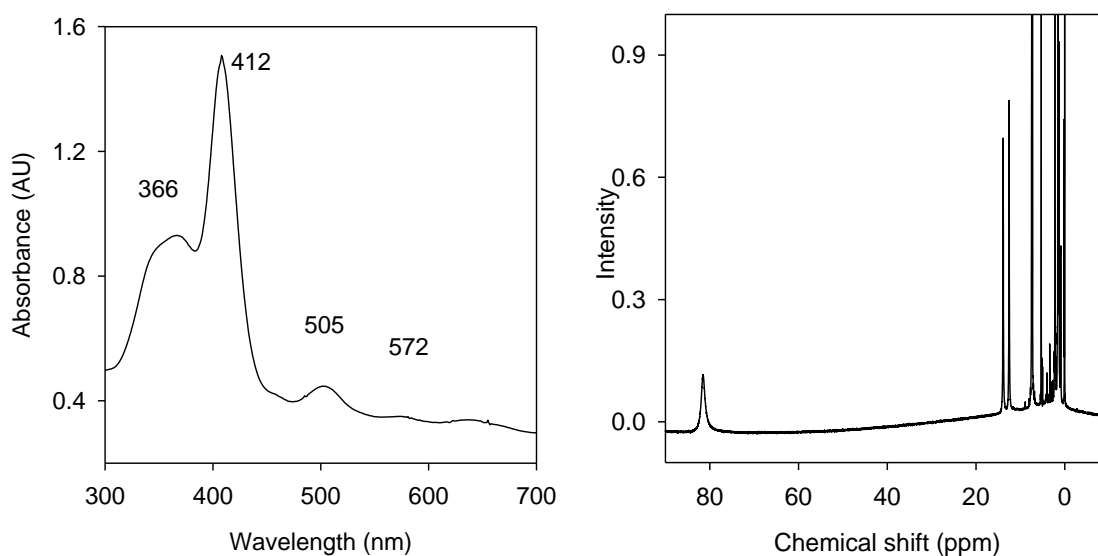


**Figure 2-4.** (A) The UV-vis spectrum of  $[\text{Fe}^{\text{III}}(\text{TDFPP})\text{Cl}]$  (**2b**) in  $\text{CH}_2\text{Cl}_2$ ; (B) The  $^1\text{H-NMR}$  spectrum of  $[\text{Fe}^{\text{III}}(\text{TDFPP})\text{Cl}]$  (**2b**) in  $\text{CDCl}_3$ .

## CHAPTER 3

### PHOTOCHEMICAL GENERATION AND KINETIC STUDIES OF HIGH-VALENT PORPHYRIN-IRON(IV)-OXO COMPOUND II MODELS

#### 3.1 Introduction

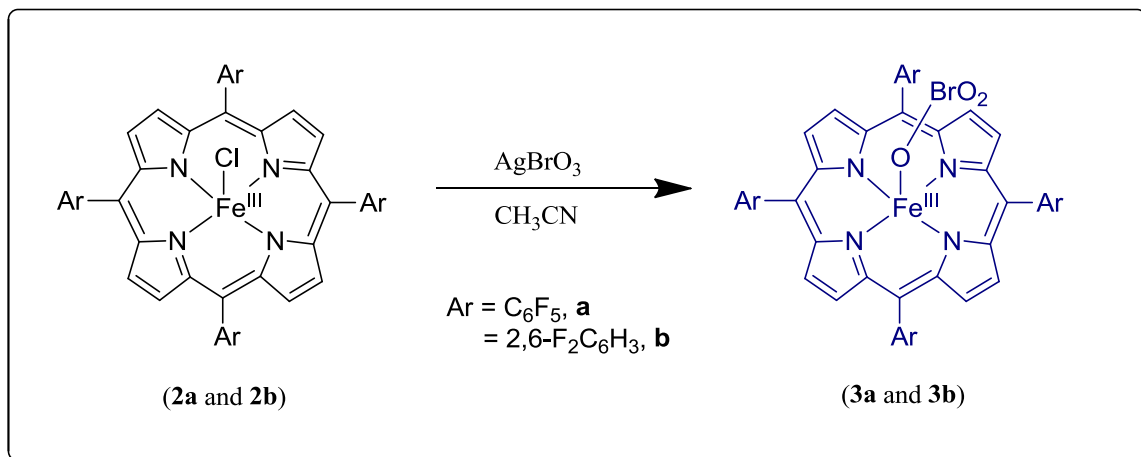
The photochemical activation of transition metal complexes to produce reactive oxidants has been known for decades.<sup>47a</sup> With the photochemical approach, reactive metal-oxo species are produced instantly, permitting direct detection of the metal-oxo species and providing one with access to time scales that are much shorter than the fastest mixing experiments for kinetic studies of their oxidation reactions.<sup>48</sup> In this regard, the photo-induced ligand cleavage reactions with visible light have been established for the formation of a variety of high-valent metal-oxo species supported by porphyrin and corrole ligands.<sup>45, 53</sup>

It had been well documented that high-valent iron(IV)-oxo porphyrin radical cations, biologically termed as compound I in heme-containing enzymes, act as the active oxidizing intermediates in catalytic cycles.<sup>32b</sup> The one-electron reduced form iron(IV)-oxo neutral porphyrin intermediates, commonly called compound II, also function as reactive species, particularly in one electron-transfer oxidations reactions such as C-H activation and hydride-transfer reactions.<sup>41-42, 54</sup> The preparation and characterization of iron(IV)-oxo radicals (compound I models) and iron(IV)-oxo neutral porphyrins (compound II models) have been known for decades now.<sup>40, 44</sup> Our particular interest in this area is to develop photochemical methods to generate and study reactive iron(IV)-oxo species in oxygen atom transfer (OAT) reactions.<sup>48</sup>

In this chapter, a new photochemical access to high-valent iron(IV)-oxo compound II models have been developed and studied.<sup>55</sup> We report rate constants for the OAT reactions of two porphyrin-iron(IV)-oxo compound II models with alkenes, activated hydrocarbons and thioanisoles in acetonitrile solution. As shown in Scheme 2-2, two tetraarylporphyrin-iron systems were studied in this work with two macrocyclic ligands **a-b**, which are generally considered as sterically encumbered porphyrins due to the presence of electron-withdrawing substituents on the *ortho* positions of the *meso* phenyl groups. The different aromatic groups on the porphyrins also result in varying electron demands, where the pentafluorophenyl system (**a**) is more electron-deficient. Iron(IV)-oxo species [Fe<sup>IV</sup>(Por)O] (**4**) were produced by visible light irradiation of highly photo-labile iron(III)-bromate complexes [Fe<sup>III</sup>(Por)(BrO<sub>3</sub>)] in anaerobic CH<sub>3</sub>CN.

## 3.2 Results and Discussion

### 3.2.1 Synthesis of Iron(III) Porphyrin Bromate Precursors



**Scheme 3-1.** Axial ligand exchange from **2a-b** to **3a-b** with  $\text{Ag}(\text{BrO}_3)$ .

As shown in Scheme 3-1, two iron(IV)-oxo porphyrins in different electronic environments were comparatively studied in this work. Facile exchange of the counterions in **2** (typically 5 mg) with excess of  $\text{Ag}(\text{BrO}_3)$  in anaerobic  $\text{CH}_3\text{CN}$  gave the corresponding bromate complexes **3**, and their formation was indicated by the UV-vis spectra as shown in Figure 3-1. These species **3** were photo-labile and subsequently prepared in situ and immediately used for photochemical reactions.

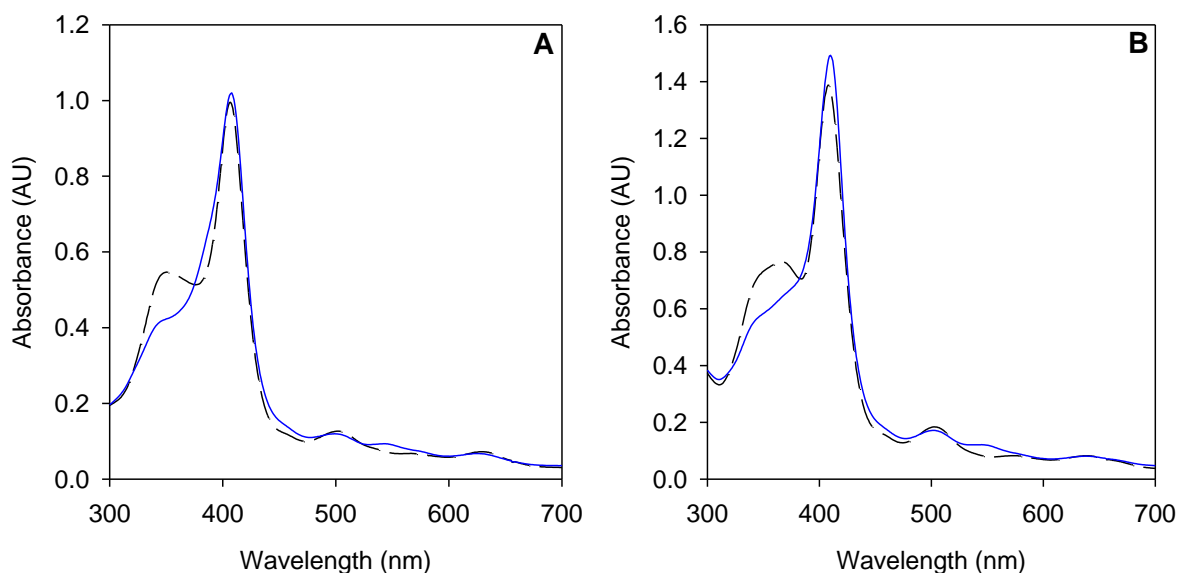


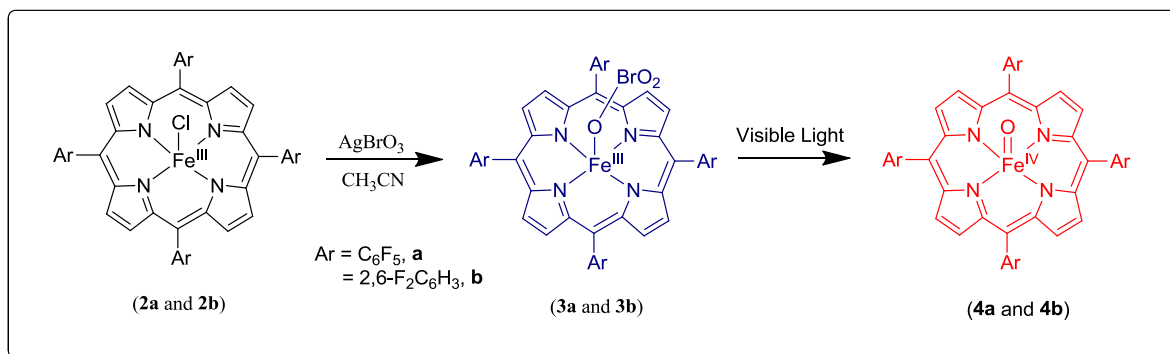
**Figure 3-1.** (A) UV-vis spectra of  $[\text{Fe}^{\text{IV}}(\text{TPFPP})\text{Cl}]$  (dashed line) and  $[\text{Fe}^{\text{III}}(\text{TPFPP})(\text{BrO}_3)]$  (solid line); (B) UV-vis spectra of  $[\text{Fe}^{\text{IV}}(\text{TDFPP})\text{Cl}]$  (dashed line) and  $[\text{Fe}^{\text{III}}(\text{TDFPP})(\text{BrO}_3)]$  (solid line).

### 3.2.2 Photo-Generation of High-Valent Iron(IV)-Oxo Porphyrins (Compound II Models)

As shown in Scheme 3-2, irradiation of bromate complexes **3a-b** in anaerobic  $\text{CH}_3\text{CN}$  with visible light from a SOLA engine (60 W) resulted in changes of the absorption spectra accompanying formation of high-valent porphyrin-iron(IV)-oxo species, i.e. compound II models in two different electron deficient porphyrins systems (**4a** and **4b**). Considering the electrophilic nature of the porphyrin-iron(IV)-oxo species, the expected order of apparent stability is  $\text{TPFPP} < \text{TDFPP}$ . The photo transformation of species **3** to **4** is characterized by a distinct color change from brown to red, accompanied by well-anchored isosbestic points at 318 nm, 485 nm, and 525 nm for **4b** (Figure 3-2 A). Correspondingly, the same oxo species **4** were also generated by chemical oxidation of



complex **2** with  $\text{PhI}(\text{OAc})_2$ , exhibiting identical spectral signature characteristic for iron(IV)-oxo porphyrins accompanied by well-anchored isosbestic points at 318 nm, 485 nm, and 525 nm (Figure 3-2 B) for **4b**.



**Scheme 3-2.** Photochemical generation of iron(IV)-oxo compound II models

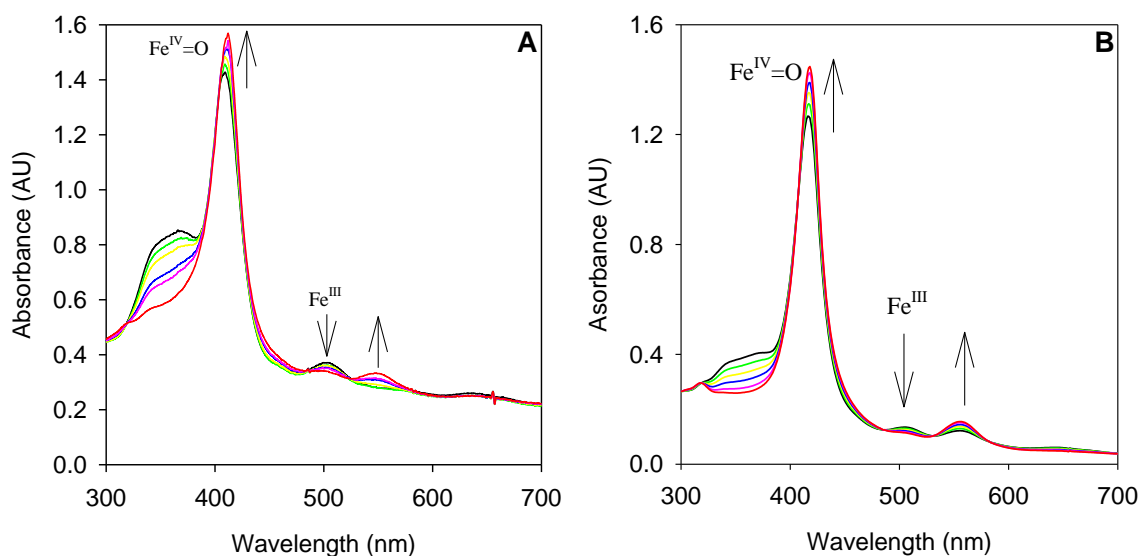
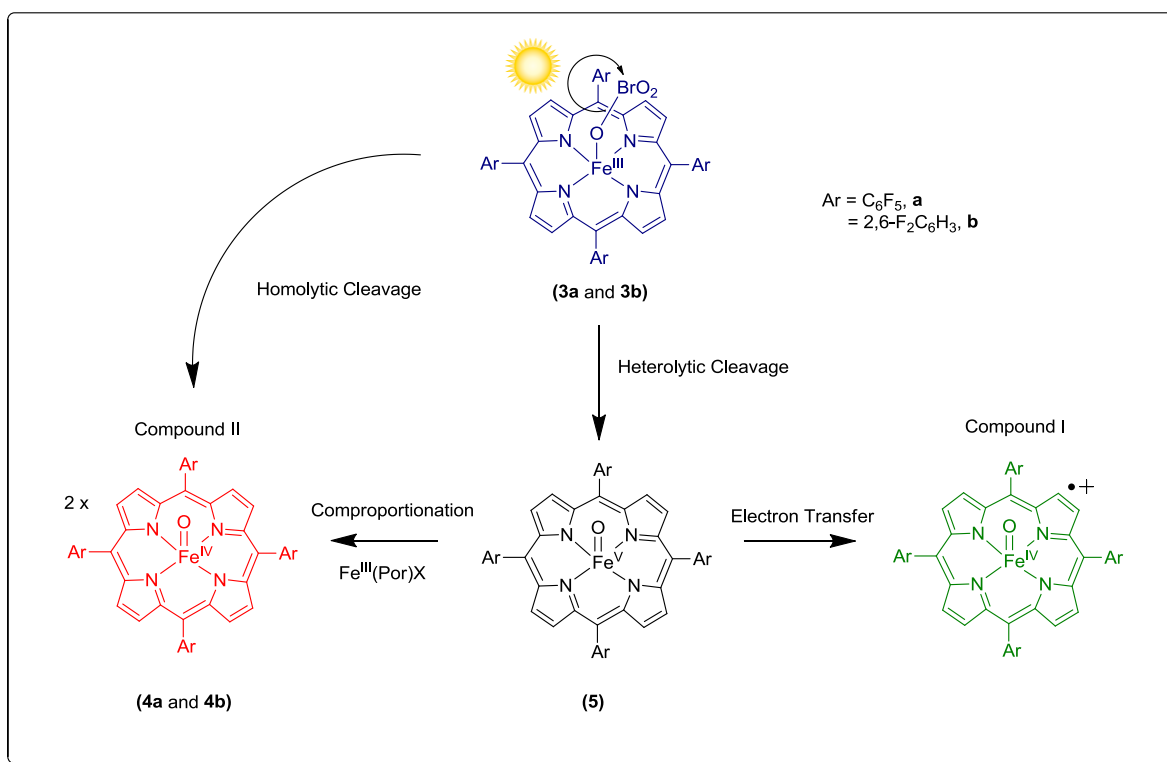


**Figure 3-2.** (A) Time-resolved spectra of **4b** following the irradiation of **3b** with visible light (120 W) in anaerobic  $\text{CH}_3\text{CN}$  solution at  $23 \pm 2^\circ\text{C}$  over 20-30 min. (B) Time-resolved spectra of **4b** following chemical oxidation of **2b** with  $\text{PhI}(\text{OAc})_2$  (5 equiv.) over 5 min.

Control experiments showed that no oxo-species **4** were formed in the absence of light. These photo-generated compound II species are relatively stable and can be isolated for further characterization.<sup>56</sup> In both cases, the formed species **4** displayed a sharper, stronger, red-shifted Soret and weaker blue-shifted Q bands that are characteristic for the corresponding porphyrin-iron(IV)-oxo derivatives. The observed photochemical formation of **4** can be simply rationalized by a homolytic cleavage of O-Br bond in the counterions of the precursor **3** (Scheme 3-3), similar to the previous work where the photochemical cleavages of porphyrin-manganese(III) chlorates gave neutral porphyrin-manganese(IV)-oxo derivatives by homolytic cleavage of the O-Cl bonds in the chlorates.<sup>57</sup>

Literature suggests that porphyrin-iron(V)-oxo species has been proposed as an alternative reactive intermediate of some heme enzymes and model systems for decades.<sup>31a</sup> In view of the decay spectra and kinetic studies of photo-generated species **4**, we propose that the photochemical formation of porphyrin-iron(IV)-oxo species may proceed via multiple pathways (Scheme 3-3). A collective body of evidence accumulated from recent reports, suggest that putative iron(V)-oxo intermediates can be involved in photochemical oxy-ligand fragmentation reactions.<sup>37, 56</sup> As thermodynamically favored, the high-valent porphyrin-iron(V)-oxo species might relax to porphyrin-iron(IV)-oxo radical cations (compound I models) by internal electron transfer (ET) from the porphyrin to the iron. However, the ET from the highly electron-deficient porphyrin to the iron sequence is apparently not favored as a result of a high redox potential or energy barrier. In view of the relatively slow formation of the iron(V)-oxo species **5** in electron-deficient

porphyrin systems, the fast comproportionation reaction of **5** with residual iron(III) complexes could result in the formation of iron(IV)-oxo derivatives, compound II. Previous studies with manganese-oxo species found that porphyrin-manganese(V)-oxo species comproportionate rapidly with manganese(III) species<sup>57</sup>, and corrole-manganese(V)-oxo species reacted with corrole manganese(III) species to give manganese(IV) species.<sup>49</sup>



**Scheme 3-3.** Mechanistic considerations on photochemical formation of iron(IV)-oxo neutral porphyrin (compound II) and iron(IV)-oxo porphyrin radical cations (compound I) controlled by the electronic nature of porphyrin ligands.

Apart from the direct homolysis of the O-Br bond, iron(IV)-oxo porphyrins can also be formed through an alternative pathway. Our previous studies showed that visible light photolysis of porphyrin-iron(III) bromates containing non-electron deficient porphyrin ligands gave porphyrin-iron(IV)-oxo radical cations (compound I models) apparently through the heterolytic cleavage of the O-Br bond in the ligand that resulted in a two-electron photo-oxidation of the iron metal.<sup>55a</sup> In contrast, the photolysis of porphyrin-iron(III) bromates with electron-deficient and sterically encumbered ligands produced compound II models. The above photolysis can be ascribed to a two-electron photo-oxidation of iron(III) precursors through heterolytic cleavages of O-Br bonds in the counterions of **3** that initially could form a putative iron(V)-oxo intermediate. Thus, the high-energy iron(V)-oxo species could quickly reduce to iron(IV)-oxo products by reacting with the solvent CH<sub>3</sub>CN. Certainly, detection and spectroscopic characterization of the initially formed intermediates at low temperature may provide more mechanistic insights into these photochemical processes. In addition, these photochemical observations can be interpreted as indicating that the electron-releasing porphyrins may favor a heterolysis of O-Br bond in the counterion, while electron-withdrawing ligands favor a homolytic reaction.

It is known that the compound II models (**4**) act as oxo-transfer agents toward various organic reductants such as alkenes and activated alkanes.<sup>56</sup> As expected, the photo-generated complexes **4** react as competent oxo-transfer agents with various sulfides such as thioanisole. In a preparative reaction, **4a** was prepared by mixing **2a** with ca. 1.5 equivalents of Ag(BrO<sub>3</sub>) in anaerobic CH<sub>3</sub>CN under visible light irradiation; the

estimated yield of **4a** determined by UV-visible spectroscopy was > 95%. A large excess of thioanisole was added, and the mixture was stirred for 5 min at ambient conditions. Following product workup, quantitative GC analysis showed the presence of a mixture of oxidized products (sulfoxide:sufone = 90:10) in > 90% yield, which was calculated based on a stoichiometry of 2 equiv of **3a** reacting with 1 equiv of the organic sulfide. Similar results were also obtained with **3b** and **3c** prepared in a same fashion. The absorption spectrum of the final complex product is consistent with that of the known porphyrin-iron(III)-hydroxo complex.<sup>58</sup>

#### **3.2.4 Kinetic Studies of Oxidations by Photo-Generated Compound II Species**

Oxidation kinetics of photo-generated iron(IV)-oxo species **4** with sulfides, alkenes, and activated hydrocarbons were investigated in this work. It is well documented that compound II models (**4**) are oxo-transfer agents with various organic reductants such as alkenes and activated alkenes.<sup>56, 59</sup> For kinetic studies, solutions containing the iron(IV)-oxo species **4** were mixed with solutions containing organic substrate at varying high concentrations, and pseudo-first-order rate constants for decay of the iron(IV)-oxo species were measured spectroscopically. Consistent with the previous studies,<sup>56</sup> we noticed that the stabilities of the porphyrin-iron(IV)-oxo species were dependent on their concentration. Therefore to circumvent uncertainties resulting from concentration effect, transients **4** with a similar concentration of approximately  $1.0 \times 10^{-5}$  M were used for all kinetic studies.<sup>56</sup>

At the low concentrations used in these kinetic studies, we found that the photo-generated species **4** were stable for hours in CH<sub>3</sub>CN solutions. The pseudo-first order decay rate constant in the absence of substrate was defined as background rate constant ( $k_0$ ). The background reaction is likely due to reaction of **4** with the solvent (CH<sub>3</sub>CN) or organic impurities. It is noteworthy that the relative rate of background decay of the oxo species **4** in CH<sub>3</sub>CN was **4b**<**4a**. In the presence of organic substrates including sulfides, alkenes, and activated hydrocarbons, the pseudo-first-order decay rate constants increased linearly with the increase of substrate concentration.

As described in the experimental section, kinetic studies were accomplished by mixing the photo-generated species **4** with organic substrates at varying high concentrations under pseudo-first-order reactions. In the presence of organic substrates, the time-resolved spectra showed a clean conversion of **4** in CH<sub>3</sub>CN to regenerate the Fe<sup>III</sup> species (Figure 3-3). In the kinetic measurements of iron(IV)-oxo porphyrins **4**, we monitored the decay of the Soret band  $\lambda_{\max}$  at 412 nm for **4a** and 415 nm for **4b** over the course of the reaction as the absorbance of the oxo **4** is stronger than that of the formed iron(III) products. The isosbestic points at 407, 430, 525, 562, and 656 nm demonstrate that the conversion of Fe<sup>IV</sup>-oxo (**4a**) to the final Fe<sup>III</sup> species does not involve the accumulation of any intermediates. The Q-band absorbance at 570 nm of the final iron(III) product is different from 505 nm of **2**, suggesting that the iron(III) porphyrin product contains hydroxide as the axial ligand, which was reported in the literature.<sup>58</sup>

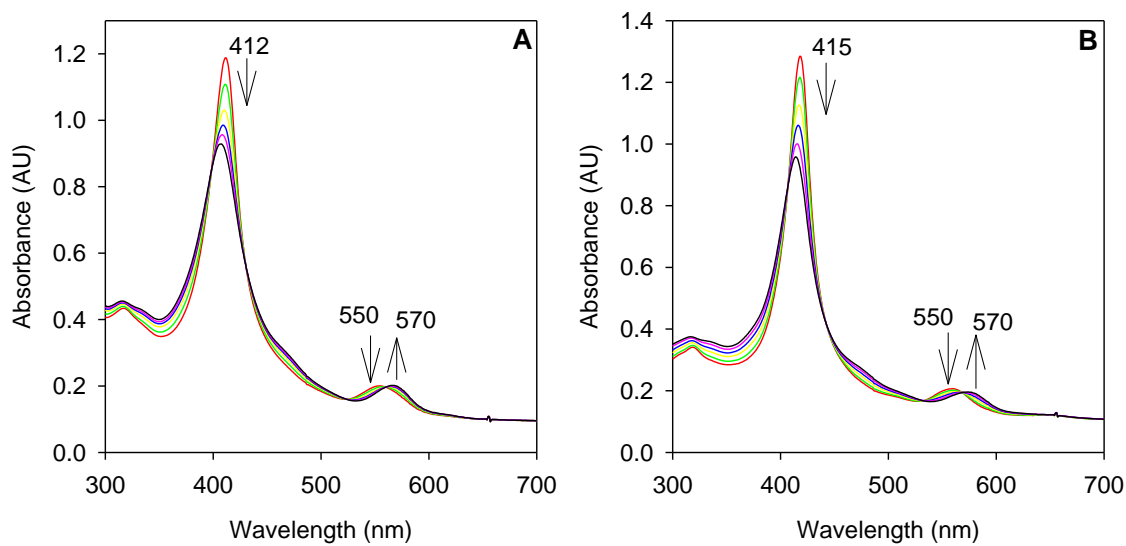


**Figure 3-3.** (A) Time resolved spectra **4a** reacting in CH<sub>3</sub>CN with ethylbenzene (0.31 M) over 140s. (B) Time resolved spectra **4b** reacting in CH<sub>3</sub>CN with ethylbenzene (0.24 M) over 140s

The kinetic plots from the reactions of **4a** and **4b** with representative organic substrates are shown graphically in Figure 3-4. Plots of  $k_{\text{obs}}$  versus the concentrations of organic substrates are linear, and the apparent second-order rate constants for oxidations with other substrates are given in Table 1. The results documented in Table 1 help one understand the difference in reactivity between the two systems. It's important to know that oxo species **4** decayed rapidly upon addition of thioanisoles, reacting as fast as 30 seconds. In Figure 3-5, we see a similar time resolved spectra demonstrating the clean conversion of **4** to iron(III) species, along with kinetic plots from the reaction of **4b** with the corresponding organic substrates, where the plots of  $k_{\text{obs}}$  versus the concentrations of thioanisoles are linear.

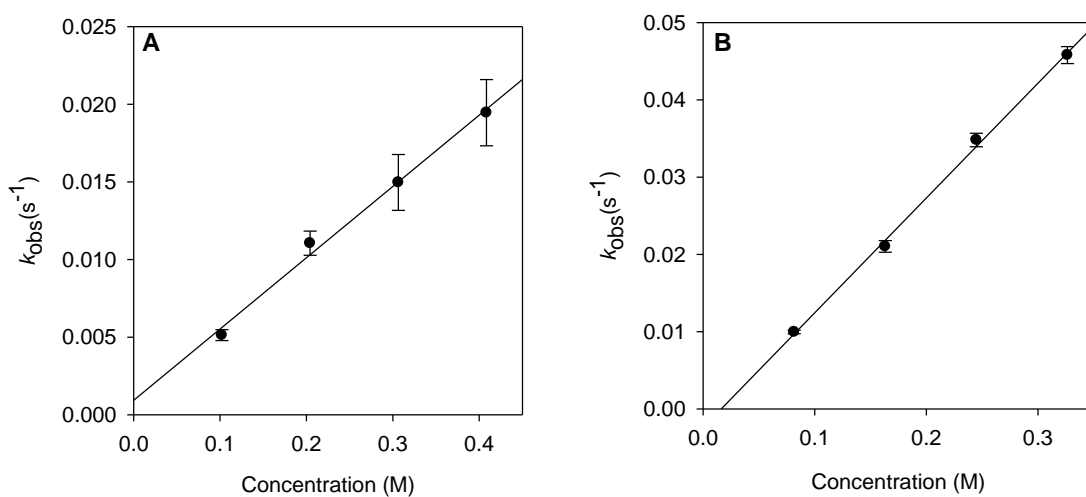


**Figure 3-4.** Kinetic plots of the observed rate constants for the reactions of **4a** (A) and **4b** (B) versus the concentrations of ethylbenzene.

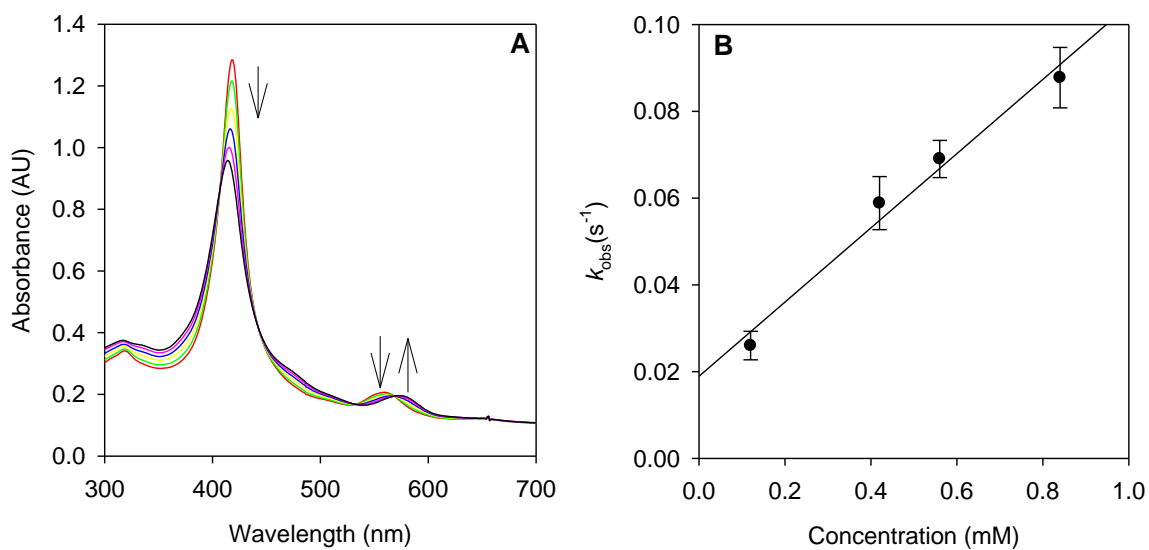


**Figure 3-5.** (A) Time resolved spectra of **4b** reacting in  $\text{CH}_3\text{CN}$  with thioanisole (0.6 mM) over 60 s. (B) Kinetic plot of the observed rate constants for the reaction of **4b** versus the concentrations of thioanisole.



**Table 3-1.** Second-order rate constants ( $k_{\text{ox}}$ ) for reactions of porphyrin-iron-oxo species **4**<sup>a</sup>

Substrate	$k_{\text{ox}}$ ( $\text{M}^{-1}\text{s}^{-1}$ )	
	[Fe <sup>IV</sup> (TPFPP)O] <b>4a</b>	[Fe <sup>IV</sup> (TDFPP)O] <b>4b</b>
<i>cis</i> -cyclooctene	$(1.6 \pm 0.2) \times 10^{-2}$	$(2.2 \pm 0.2) \times 10^{-2}$
cyclohexene	$(6.3 \pm 0.2) \times 10^{-2}$	$(8.3 \pm 0.5) \times 10^{-2}$
<i>cis</i> -stilbene	$(6.1 \pm 0.4) \times 10^{-3}$	$(4.9 \pm 0.6) \times 10^{-2}$
ethylbenzene	$(4.6 \pm 0.3) \times 10^{-2}$	$(1.5 \pm 0.1) \times 10^{-1}$
ethylbenzene- <i>d</i> <sub>10</sub>	$(1.7 \pm 0.1) \times 10^{-3}$	$(2.5 \pm 0.4) \times 10^{-2}$
thioanisole	$(4.6 \pm 0.2) \times 10^1$	$(8.6 \pm 1.8) \times 10^1$
<i>p</i> -fluorothioanisole	$(2.6 \pm 0.5) \times 10^1$	$(5.0 \pm 0.3) \times 10^1$
<i>p</i> -chlorothioanisole	$(5.5 \pm 0.7) \times 10^1$	$(8.7 \pm 0.4) \times 10^1$
<i>p</i> -methylthioanisole	$(6.9 \pm 1.1) \times 10^1$	$(1.1 \pm 0.1) \times 10^2$
<i>p</i> -methoxythioanisole	$(8.1 \pm 1.5) \times 10^1$	$(2.0 \pm 0.2) \times 10^2$
styrene	$(7.7 \pm 0.1) \times 10^{-3}$	$(1.5 \pm 0.1) \times 10^{-2}$
<i>p</i> -chlorostyrene	$(7.2 \pm 0.2) \times 10^{-3}$	$(3.7 \pm 0.6) \times 10^{-2}$
<i>p</i> -fluorostyrene	$(8.4 \pm 0.1) \times 10^{-3}$	$(1.6 \pm 0.1) \times 10^{-2}$
<i>p</i> -methylstyrene	$(8.5 \pm 0.8) \times 10^{-3}$	$(2.4 \pm 0.1) \times 10^{-2}$
<i>p</i> -methoxystyrene	$(5.3 \pm 0.3) \times 10^{-2}$	$(7.9 \pm 0.4) \times 10^{-2}$
1-phenylethanol	$(3.7 \pm 0.1) \times 10^{-2}$	$(9.8 \pm 0.3) \times 10^{-2}$
diphenylmethane	$(1.7 \pm 0.1) \times 10^{-2}$	$(4.7 \pm 0.1) \times 10^{-2}$
diphenylmethanol	$(4.9 \pm 0.4) \times 10^{-2}$	$(9.3 \pm 0.9) \times 10^{-1}$

<sup>a</sup> In CH<sub>3</sub>CN at 23 ± 2 °C. The values are average of 2-3 runs with 2σ standard deviation.

Of note, from the tabulated results one can conclude that the organic sulfides are about 3 to 4 orders of magnitude more reactive than alkenes, ethylbenzene, *para*-substituted styrenes, and benzyl alcohols with the same oxo species. The second-order rate values determined in this study provide a quantitative measure of the rate acceleration of sulfide oxidation by compound II models. The assessment of the available kinetic data in Table 1 point out that organic sulfides are most reactive, with second-order rate constants ( $k_{\text{ox}}$ ) ranging from  $(2.0 \pm 0.2) \times 10^2$  to  $(2.6 \pm 0.5) \times 10^1 \text{ M}^{-1}\text{s}^{-1}$ . In the well-studied alkene epoxidations and activated C-H bond oxidations by the same oxo species, the  $k_{\text{ox}}$  values obtained under identical conditions as these reactions are in the ranges of  $(7.9 \pm 0.4) \times 10^{-2}$  to  $(6.1 \pm 0.4) \times 10^{-3}$  (epoxidation) and  $(9.3 \pm 0.9) \times 10^{-1}$  to  $(3.7 \pm 0.2) \times 10^{-2} \text{ M}^{-1}\text{s}^{-1}$  (hydroxylation). Hence, the rate acceleration for sulfide oxidations by the oxo-species **4** clearly reflects the enhanced nucleophilicity, and propensity of sulfur for oxidation versus hydrocarbons. Furthermore, the oxidations of the *para*-substituted thioanisoles provide insights into the electronic demands of the transition states of the oxidation reactions. In both the systems studied here, we observe a relatively narrow substitute dependence in the second-order rate constants for the *para*-substituted thioanisoles. Figure 3-6(A) shows representative kinetic data from the reaction of *para*-substituted thioanisoles with **4a**, which results in a non-linear Hammett Correlation curve with  $\sigma^+$  substituent values, Figure 3-6(B).

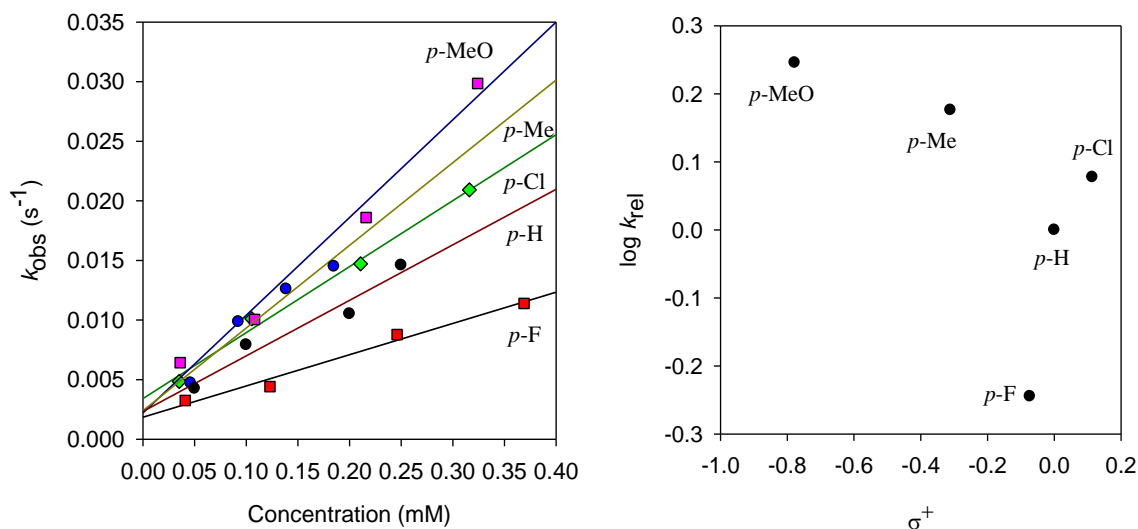


**Figure 3-6.** (A) Plots of the observed pseudo-first-order rate constants versus different concentrations of thioanisole with **4a**. (B) Linear free-energy relationship for rate constants for reactions of **4a** with thioanisoles with  $\sigma^+$  values.

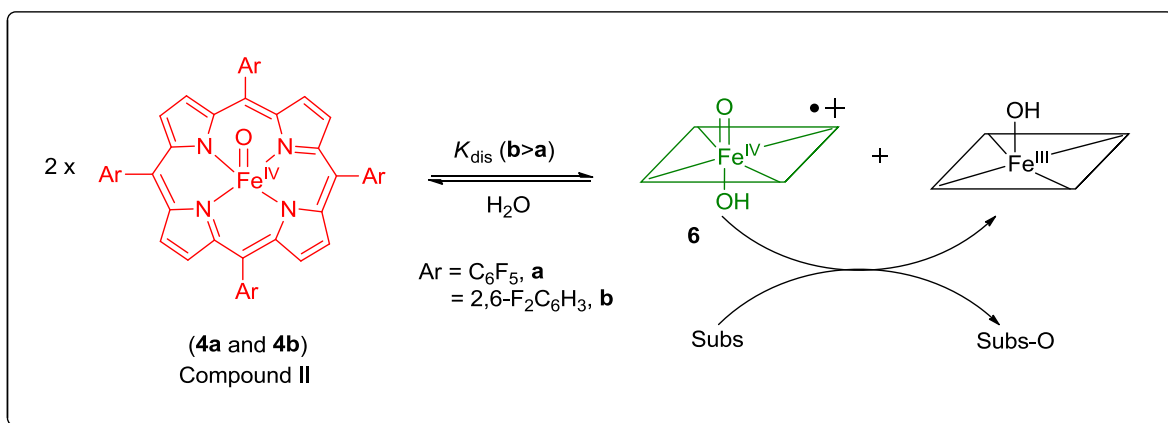
The Hammett analysis results suggest that no considerable charge develops on the sulfur during the oxidation process with compound II species. Similarly, non-linear Hammett plots have also been observed for the reactions of *para*-substituted styrenes and benzyl alcohols with compound II species, which were ascribed to substantial development of radical character on the benzylic carbon in the transition state.<sup>56, 60</sup> Upon comparison of the second-order rate constants from Table 1 for the iron(IV)-oxo porphyrin **4**, we can see that an inverted reactivity pattern for iron(IV)-oxo porphyrin **4** with all substrates is observed (see later discussion). The  $k_{\text{ox}}$  values reported in Table 1 for alkenes are in good agreement with the previously reported values for oxidant **4** produced by the chemical oxidation method.<sup>56</sup> Specifically, it is known in the literature that alkene epoxidation by the same compound II oxidants typically proceeds via rate-

limiting formation of an iron porphyrin-bound benzylic radical intermediate.<sup>60</sup> Interestingly, it is observed in Table 1 that the rate constants for the reactions of ethylbenzene are unusually larger than those for the reactions of alkenes, presumably reflecting the operation of a different mechanism worth investigating in the near future.

### 3.2.5 Mechanistic Consideration on the Reaction of Photo-Generation of Compound II

Owing to the electrophilic nature of high-valent metal-oxo species, one typically observes that more electron-withdrawing ligands give more reactive metal-oxo derivatives.<sup>62</sup> For the two porphyrins systems studied here, however, the reactivity order is inverted, with the system of less electron demand, i.e. the TDFPP complex **4b** apparently reacting faster with any given substrate than the more electron-deficient **4a** complex. In view of the similar structure and similar photochemical and spectral behaviors for **4a** and **4b**, the different reactivities do not result from operation of different mechanisms in their oxidation reactions. Certainly, these kinetic results strongly support the previously proposed mechanistic model involving disproportionation of **4** to give Fe<sup>III</sup> and a more reactive porphyrin-iron(IV)-oxo radical cationic species **6** as the predominant oxidants in these systems (Scheme 3-4).<sup>56, 60</sup>

In practice, the concentration of **6** might be too small to permit detection, hence the major species observed spectroscopically is still **4**. The equilibrium reactions of species **6** should be more favorable if they are the actual oxidants, especially for a less electron demanding system. Accordingly, the observed kinetics could reflect the populations of species **4** controlled by a disproportionation equilibrium constant ( $K_{\text{dis}}$ ), which should be larger for the less electron-demanding TDFPP ligand. Furthermore, oxidation by a higher valence state (+5) form than species **4** (+4) also provides a convenient “two-electron” oxo transfer reagent that can oxidize substrate with the formation of an iron(III) product instead of iron(II) (Scheme 3-4). It should be pointed out that even if a direct OAT from the Fe(IV)=O species to substrate did occur, it is unlikely that sufficient Fe(II) would accumulate to be observable under the reaction conditions.



**Scheme 3-4.** A disproportionation pathway for reactions of species **4**.

The mechanistic model in Scheme 3-4 is similar to that proposed for reactions of neutral porphyrin–manganese(IV)-oxo and corrole–manganese(V)-oxo species<sup>49, 53a</sup> where the actual oxidants in those two systems are apparently cationic porphyrin–

manganese(V)-oxo and corrole-manganese(VI)-oxo species, respectively, formed via a disproportionation mechanism. Hence, we propose a disproportionation reaction where the iron(IV)-oxo species disproportionates to give an iron(III) species and a more reactive oxoiron(IV) porphyrin radical cation that is the true oxidant.<sup>56, 63</sup> This conclusion is supported by the inverted reactivity pattern in regard to the electron demand of the porphyrin ring.

Importantly, direct conversion of **4** to the compound I species **6** in an acid-catalyzed reaction has been reported.<sup>63</sup> This disproportionation mechanism provides a clear explanation of previous research results in that compound II species are more stable in alkaline solutions than in neutral or acidic solutions, owing to slow formation of reactive compound I in the absence of acid catalyst. Despite that, further support of the mechanism proposed in Scheme 3-4 is the suppression of the rate of reaction of iron(IV)-oxo porphyrin species with thioanisole as a function of decrease in concentration of iron(IV)-oxo porphyrin species **4**. From a series of kinetic experiments conducted, on decreasing the concentration of **4** by changing the concentration of the precursor **3**, the apparent pseudo-first-order rate constant for reaction of **3** in presence of 4.0 mM thioanisole were measured. The observed rate constants decreased as the concentration of **4** decreased (Figure 3-7).

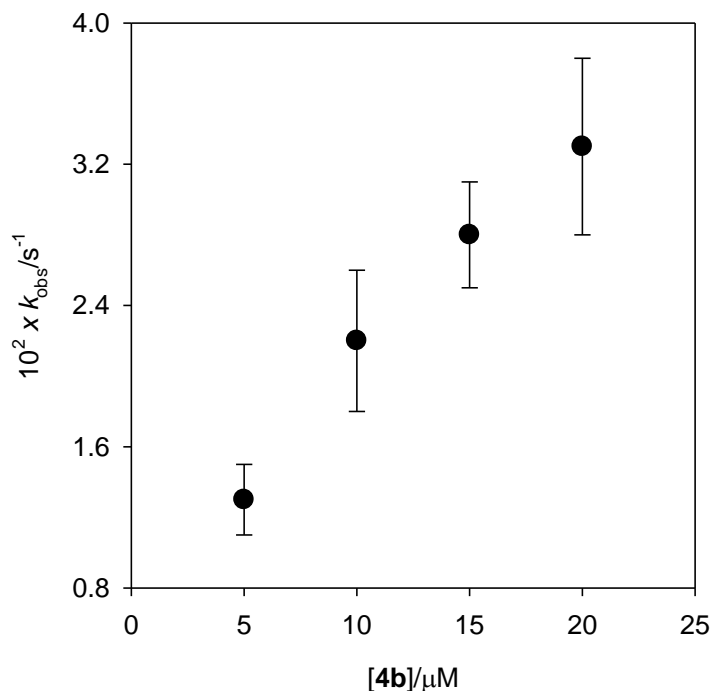


**Figure 3-7.** Observed apparent pseudo-first-order rate constants for reaction of **4b** in  $\text{CH}_3\text{CN}$  in the presence of 4.0 mM thioanisole. The concentrations of precursor **3b** are listed under the photochemical conditions used in this study; the conversion of **3b** to **4b** was > 95%.

The observed concentration effects for reactions of **4** with substrates mirrored those found for decreased life-time of **4** in NMR experiments. The disproportionation reaction rate would increase significantly at higher concentration of **4** used in NMR experiments (ca. 5 mM), thus the life-time of **4** decreased to a few minutes.<sup>56</sup> In contrast, the dilute samples of **4** in  $\text{CH}_3\text{CN}$  used for the kinetic studies (ca. 10  $\mu\text{M}$ ) were stable for hours.

Although most experimental results in this work can be explained by the disproportionation pathway, it does not provide the only explanation for the inverted reactivity patterns found for the photo-generated iron(IV)-oxo porphyrin systems studied here. In view of the much enhanced nucleophilicity of sulfide substrates, compound II could function as a direct OAT agent where the oxygen transfer occurs from iron to sulfides with a possible radical intermediate. This premise is supported by a similar pathway proposed for epoxidation of alkenes by compound I species.<sup>64</sup> In this way, an iron(II) porphyrin could be formed, and then rapidly undergo aerobic oxidation to generate the observed iron(III) hydroxyl product through an iron(III)-(O<sub>2</sub>)<sup>-</sup> intermediate.<sup>65</sup> The other explanation for the inverted order of reactivity towards oxygen transfer from the iron(IV)-oxo species, results from the availability of the decreased electron density for equatorial binding in more electron-withdrawing porphyrins with a possibility of a tighter binding of axial ligands.<sup>66</sup> The comprehensive kinetic studies provide mechanistic insights as to the identity and reactivity of the active oxidant in the catalytic oxidations. The results generate a fundamental data set for the kinetics of reactions of P450 compound II models. This in turn permits comparisons of the absolute rate constants of sulfoxidations with rate constants of well-known epoxidation and hydroxylation reactions toward the same metal-oxo species.



## CHAPTER 4

### CONCLUSION

In conclusion, the studies reported here have demonstrated that visible light photolysis of the photo-labile iron(III) bromate complexes efficiently produce high-valent iron(IV)-oxo model derivatives, which exhibit a marked effect on the structure and substituents of porphyrin ligands. Iron(IV)-oxo neutral porphyrins compound II models are produced in sterically hindered and electron-deficient systems. These observations implied that the above photolyses involve a heterolytic cleavage of O-Br in precursors **3** to generate a putative iron(V)-oxo intermediate, which might relax to compound I through ET from porphyrin to the iron, or undergo the rapid comproportionation reaction with residual iron(III) to afford a compound II derivative. The kinetics of alkene, activated hydrocarbon and sulfide oxidation reactions by photo-generated porphyrin-iron(IV)-oxo complexes was conducted in two electron-deficient systems. This study reveals the sulfide oxidation reactions are 3 to 4 orders of magnitude faster than those of the well-studied epoxidation and activated C-H bond hydroxylation reactions. The order of reactivity for the iron(IV)-oxo porphyrins in the oxidation of all substrates are inverted from those expected for electrophilic metal-oxo oxidants. These observations indicate the oxidation reactions by these compound II models presumably react through a disproportionation mechanism to generate higher oxidized iron-oxo species as the true oxidant, similar to those in reactions of alkenes and alcohols. Conventional Hammett analyses with a  $\sigma^+$  values gave a non-linear correlation, indicating no significant charge develops at the sulfur atoms. Indeed, the more reactive iron(IV)-oxo radical cation is

indicated as the principal reactive intermediate, even though it was not observed during the catalytic reaction.

## REFERENCES

1. (a) Sheldon, R. A., *Metalloprophyrins In Catalytic Oxidations*. Marcel Dekker: New York, 1994; (b) Ortiz de Montellano, P. R., *Cytochrome P450 Structure, Mechanism, and Biochemistry*. 3rd ed.; Kluwer Academic/Plenum: New York, 2005.
2. (a) Caron, S.; Dugger, R. W.; Ruggeri, S. G.; Ragan, J. A.; Ripin, D. H. B., Large-Scale Oxidations in the Pharmaceutical Industry. *Chem. Rev.* **2006**, *106*, 2943-2989; (b) Shilov, A. E.; Shulpin, G. B., Activation of C-H bonds by metal complexes. *Chem. Rev.* **1997**, *97* (8), 2879-2932; (c) Brink, G. T., Green, Catalytic Oxidation of Alcohols in Water. *Science* **2000**, *287* (5458), 1636-1639; (d) Groves, J. T., Shalyaev, K.; Lee, J., Oxometalloporphyrins in Oxidative Catalysis. In *The Porphyrin Handbook*, Kadish, K. M. S., K. M.; Guillard, R., Ed. 2000; Vol. 4, pp 17-40.
3. (a) Punniyamurthy, T.; Velusamy, S.; Iqbal, J., Recent Advances in Transition Metal Catalyzed Oxidation of Organic Substrates with Molecular Oxygen. *Chem.Rev.* **2005**, *105* (6), 2329-2363; (b) Zhang, R.; Vanover, E.; Chen, T.-H.; Thompson, H., Visible light-driven aerobic oxidation catalyzed by a diiron(IV)  $\mu$ -oxo biscorrole complex. *Appl. Catal. A* **2013**, *465*, 95-100.
4. Zhang, R., Asymmetric Organic Oxidation by Chiral Ruthenium Complexes Containing D<sub>2</sub>- and D<sub>4</sub>- Symmetric Porphyrinato Ligands. *Ph. d. Thesis* **2000**, 1-235.
5. Axelrod, J., The enzymatic demethylation of ephedrine. *J. of Pharma.* **1955**, *114*, 430-438.
6. (a) Guengerich, P. F., Common and Uncommon Cytochrome P450 Reactions Related to Metabolism and Chemical Toxicity. *Chem. Res. in Tox.* **2001**, *14* (6), 611-650;

- (b) Chang, Y. T.; Loew, G. H., Construction and evaluation of a three-dimensional structure of cytochrome P450choP enzyme (CYP105C1). *peps* **1996**, *9*, 755-766.
7. Sono, M.; Roach, M. P.; Coulter, E. D.; Dawson, J. H., Heme-Containing Oxygenases. *Chem. Rev.* **1996**, *96* (7), 2841-2887.
8. (a) Meunier, B., *Metal-Oxo and Metal-Peroxo Species in Catalytic Oxidations*. Springer-Verlag: Berlin, 2000; (b) Garfinkel, D., Studies on pig liver microsomes. I. enzymic and pigment composition of different microsomal fractions. *Archives of Biochemistry and Biophysics* **1958**, *77*, 493-509; (c) Klingenberg, M., Pigments of rat liver microsomes. *Archives of Biochemistry and Biophysics* **1958**, *75*, 376-386.
9. (a) Omura, T. S., R., The carbon monoxide-binding pigment of liver microsomes. I. Evidence for its hemoprotein nature. *J. Bio. Chem.* **1964**, *239*, 2370-2378; (b) Omura, T. S., R., The carbon monoxide-binding pigment of liver microsomes. II. solubilization, purification and properties. *J. Bio. Chem.* **1964**, *239*, 2378-2385.
10. Mueller, E. J.; Loida, P. G.; Sligar, S. G., Twenty-five years of P450<sub>cam</sub> research. *Cytochrome P450: Structure, Function and Biochemistry* **1995**, 83-124.
11. Guengerich P. F., Intersection of Roles of Cytochrome P450 Enzymes with Xenobiotic and Endogenous Substrates. Relevance to Toxicity and Drug Interactions. *Chem. Res. in Tox.* **2017**, *30* (1), 2-12.
12. Denisov, I. G.; Makris, T. M.; Sligar, S. G.; Schlichting, I., Structure and chemistry of cytochrome P 450. *Chem. Rev.* **2005**, *105* (6), 2253-2277.
13. Ruckpaul, K. R., H., Cytochrome P450. *Volker Ulrich* **1986**, *25* (3), 294.

14. Roberts, G. A., ; Grogan, G.; Greter, A.; Flitsch, S, L.; Turner, N, J.,; Identification of a New Class of Cytochrome P450 from a Rhodococcus sp. *J. Bact.* **2002**, *184* (14), 3898-3908.
15. Maurer, S. C. S., H.; Schmid, R. D.; Urlacher, V., Immobilisation of P450BM-3 and an NADP(+) cofactor recycling system: Towards a technical application of heme-containing monooxygenases in fine chemical synthesis. *Adv. Syn. Cat.* **2003**, *345*, 802.
16. (a) Wilkinson, G. R., Drug Metabolism and Variability among Patients in Drug Response. *N. Engl. J. Med.* **2005**, *352* (21), 2211-2221; (b) Slaughter, R. L. Edwards, D. J.; Recent Advances: the cytochrome P450 enzymes. *Ann Pharmacother* **1995**, *29* (6), 619-624.
17. Lynch, T. P., A., The effect of cytochrome P450 metabolism on drug response, interaction, and adverse effects. *Am. Fam. Physician* **2007**, *76* (3), 391-396.
18. Poulos, T. L. F., B. C.; Gunsalus, I. C.; Wagner G. C.; Kraut, J., The 2,6-A crystal structure of Pseudomonas putida cytochrome P-450. *J. Bio. Chem.* **1985**, *260*, 16122.
19. (a) Poulos, T. L. F., B. C.; Howard, A. J.; , Crystal Structure of Substrate-Free Pseudomonas Putida Cytochrome P450. *J. Biochem.* **1986**, *25*, 5314-5322; (b) Poulos, T. L. F., B. C.; Howard, A. J., High-Resolution Crystal Structure of Cytochrome P450<sub>cam</sub>. *J Mol. Bio.* **1987**, *195*, 687-700.
20. Groves, J. T., Reactivity and Mechanisms of Metalloporphyrin-Catalyzed Oxidations. *J. Porph. Phthal* **2000**, *4*, 350-352.
21. Meunier, B., Metalloporphyrins as Versatile Catalysts for Oxidation Reactions and Oxidative DNA Cleavage. *Chem. Rev.* **1992**, *92* (6), 1411-1456.

22. Groves, J. T. N., T. E.; Myers, R. S.; Hydroxylation and Epoxidation Catalyzed by Iron-Porphyrin Complexes. Oxygen Transfer from Iodosylbenzene. *J. Am. Chem. Soc.* **1979**, *101*, 1032-1033.
23. Rose, E.; Andrioletti, B.; Zrig, S.; Quelquejeu-Etheve, M., Enantioselective epoxidation of olefins with chiral metalloporphyrin catalysts. *Coord. Chem. Rev.* **2005**, *34*, 573-583.
24. Davies, J. A., *Selective Hydrocarbon Activation: Principle and Progress*. VCH New York, 1994.
25. Perree-Fauvet, M.; Gaudemer, A., Manganese porphyrin-catalyzed oxidation of olefins to ketones by molecular oxygen. *Chem. Commun.* **1981**, (17), 874-875.
26. Battioni, P.; Renaud, J. P.; Bartoli, J. F.; Reina-Artiles, M.; Fort, M.; Mansuy, D., Monooxygenase-like oxidation of hydrocarbons by hydrogen peroxide catalyzed by manganese porphyrins and imidazole: selection of the best catalytic system and nature of the active oxygen species. *J. Am. Chem. Soc.* **1988**, *110*, 8462-8470.
27. Mansuy, D., Activation of alkanes: the biomimetic approach. *Coord. Chem. Rev.* **1993**, *125*, 129-142.
28. (a) Groves, J. T. K., William J., Jr.; Haushalter, Robert C., Hydrocarbon oxidations with oxometalloporphyrins. Isolation and reactions of a (porphinato)manganese(V) complex. *J. Am. Chem. Soc.* **1980**, *102* (20), 6375-7; (b) Hill, C. L.; Schardt, B. C., Alkane activation and functionalization under mild conditions by a homogeneous manganese(III)porphyrin-iodosylbenzene oxidizing system. *J. Am. Chem. Soc.* **1980**, *102* (20), 6374-5; (c) Groves, J. T.; Lee, J.; Marla, S. S., Detection and

Characterization of an Oxomanganese(V) Porphyrin Complex by Rapid-Mixing Stopped-Flow Spectrophotometry. *J. Am. Chem. Soc.* **1997**, *119* (27), 6269-6273.

29. Abebrese, C.; Huang, Y.; Pan, A.; Yuan, Z.; Zhang, R., Kinetic studies of oxygen atom transfer reactions from trans-dioxoruthenium(VI) porphyrins to sulfides. *J. Inorg. Biochem.* **2011**, *105*, 1555-1561.

30. (a) Baglia, R. A. Z., J. P.; Goldberg, D. P.; Biomimetic Reactivity of Oxygen-Derived Manganese and Iron Porphyrinoid Complexes. *Chem. Rev.* **2017**, *117* (21), 13320-13352; (b) Wallar, B. J.; Lipscomb, J. D., Dioxygen activation by enzymes containing binuclear non-heme iron clusters. *Chem. Rev.* **1996**, *96* (7), 2625-2657.

31. (a) Fujii, H., Electronic structure and reactivity of high-valent oxo iron porphyrins. *Coord. Chem. Rev.* **2002**, *226*, 51-60; (b) Costas, M.; Mehn, M. P.; Jensen, M. P.; Que, L., Dioxygen Activation at Mononuclear Nonheme Iron Active Sites: Enzymes, Models, and Intermediates. *Chem. Rev.* **2004**, *104*, 939-986; (c) Nam, W., High-Valent Iron(IV)-Oxo Complexes of Heme and Non-Heme Ligands in Oxygenation Reactions. *Acc. Chem. Res.*, **2007**, *40* (7), 522-531; (d) de Visser, S. P.; Nam, W., High-valent iron-oxo porphyrins in oxygenation reactions. In *Handbook of Porphyrin Science*, Kadish, K. M.; Smith, K. M.; Guilard, R., Eds. World Scientific Publishing: Singapore, 2010; Vol. 10, pp 85-139; (e) McDonald, A. R.; Que, L., High-valent nonheme iron-oxo complexes: Synthesis, structure, and spectroscopy. *Coord. Chem. Rev.* **2013**, *257*, 414-428.

32. (a) Rutter, R.; Hager, L. P.; Dhonau, H.; Hendrich, M.; Valentine, M.; Debrunner, P., Chloroperoxidase compound I: electron paramagnetic resonance and Moessbauer

- studies. *Biochem.* **1984**, *23*, 6809; (b) Dawson, J. H., Probing structure-function relations in heme-containing oxygenases and peroxidases. *Science* **1988**, *240* (4851), 433-9.
33. Zamocky, M.; Furtmüller, P. G.; Obinger, C., Evolution of catalases from bacteria to humans. *Antioxid. Antioxid Redox Signal* **2008**, *10*, 1527-1548.
34. (a) Tiago de Oliveira, F.; Chanda, A.; Banerjee, D.; Shan, X.; Mondal, S.; Que, L., Jr.; Bominaar, E. L.; Muenck, E.; Collins, T. J., Chemical and Spectroscopic Evidence for an FeV-Oxo Complex. *Science* **2007**, *315* (5813), 835-838; (b) Ghosh, M.; Singh, K. K.; Panda, C.; Weitz, A.; Hendrich, M. P.; Collins, T. J.; Dhar, B. B.; Gupta, S., Formation of a Room Temperature Stable FeV(O) Complex: Reactivity Toward Unactivated C–H Bonds. *J. Am. Chem. Soc.* **2014**, *136*, 9524-9527.
35. (a) Kellner, D. G.; Hung, S.-C.; Weiss, K. E.; Sligar, S. G., Kinetic characterization of compound I formation in the thermostable cytochrome P450 CYP119. *J. Biol. Chem.* **2002**, *277*, 9641; (b) Rittle, J.; Green, M. T., Cytochrome P450 Compound I: Capture, Characterization, and C-H Bond Activation Kinetics. *Science* **2010**, *330*, 933-937.
36. Dey, A.; Ghosh, A., "True" iron(V) and iron(VI) porphyrins: a first theoretical exploration. *J. Am. Chem. Soc.* **2002**, *124* (13), 3206-7.
37. (a) Harischandra, D. N.; Zhang, R.; Newcomb, M., Photochemical Generation of a Highly Reactive Iron-Oxo Intermediate. A True Iron(V)-Oxo Species? *J. Am. Chem. Soc.* **2005**, *127* (40), 13776-13777; (b) Pan, Z.; Wang, Q.; Sheng, X.; Horner, J. H.; Newcomb, M., Highly Reactive Porphyrin–Iron–Oxo Derivatives Produced by Photolyses of Metastable Porphyrin–Iron(IV) Diperochlorates. *J. Am. Chem. Soc.* **2009**, *131* (7), 2621-2628.



38. Jung, C. S.; V. Lenzian, F., Freeze-quenched iron-oxo intermediates in cytochromes P450. *Biochem. Biophys. Res. Commun.* **2005**, *338*, 355-364.
39. (a) Pan, Z.; Zhang, R.; Fung, L. W. M.; Newcomb, M., Photochemical Production of a Highly Reactive Porphyrin-Iron-Oxo Species. *Inorg. Chem.* **2007**, *46* (5), 1517-1519;  
(b) Watanabe, Y.; Fujii, H., Characterization of High-Valent Oxo-Metalloporphyrins. In *Metal-Oxo and Metal-Peroxo Species in Catalytic Oxidations*, Meunier, B., Ed. Springer-Verlag: Berlin, 2000.
40. Groves, J. T.; Haushalter, R. C.; Nakamura, M.; Nemo, T. E.; Evans, B. J., High-valent iron-porphyrin complexes related to peroxidase and cytochrome P-450. *J. Am. Chem. Soc.* **1981**, *103* (10), 2884-6.
41. (a) Green, M. T.; Dawson, J. H.; Gray, H. B., Oxoiron(IV) in Chloroperoxidase Compound II Is Basic: Implications for P450 Chemistry. *Science* **2004**, *304*, 1653-1656;  
(b) Rutkowska-Zbik, D. D.-M., A.; Witko, M., The Influence of Structural Parameters on the Reactivity of Model Complexes for Compound II: A Mini Review. *Top. Catal.* **2014**, *57* (10-13), 946-952.
42. (a) Nam, W.; Park, S. E.; Lim, I. K.; Lim, M. H.; Hong, J.; Kim, J., First direct evidence for stereospecific olefin epoxidation and alkane hydroxylation by an oxoiron(IV) porphyrin complex. *J. Am. Chem. Soc.* **2003**, *125*, 14674-14675; (b) Fertinger, C. H.-I., N.; Franke, A.; van Eldik, R., Direct comparison of the reactivity of model complexes for Compounds 0, I, and II in oxygenation, hydrogen-abstraction, and hydride-transfer processes. *Chem Eur. J.* **2009**, *15* (48), 13435-13440.
43. (a) Fujii, H. Y., T.; Kamada, H., ESR Studies of A<sub>1u</sub> and A<sub>2u</sub> Oxoiron(IV) Porphyrin  $\pi$ -Cation Radical Complexes. Spin Coupling between Ferryl Iron and A<sub>1u</sub>/A<sub>2u</sub>

- Orbitals. *Inorganic Chem* **1995**, *35* (8), 2373-2377; (b) Kincaid, J. R. S., A. J.; Paeng, K. J., The resonance Raman spectrum of a ferrylporphyrin cation radical and its photodegradation in the presence of methanol. *J. Am. Chem. Soc.* **1989**, *111* (2), 735-737.
44. Chin, D.-H.; La Ma., G. N.; Balch, A. L., Role of ferryl (FeO<sub>2</sub><sup>+</sup>) complexes in oxygen atom transfer reactions. Mechanism of iron(II) porphyrin catalyzed oxygenation of triphenylphosphine. *J. Am. Chem. Soc.* **1980**, *102*, 5945-5947.
45. Chen, T. H.; Asiri, N.; Kwong, K. W.; Malone, J.; Zhang, R., Ligand control in the photochemical generation of high-valent porphyrin-iron-oxo derivatives. *Chem. Commun.* **2015**, *51*, 9949-9952.
46. Maldotti, A.; Molinari, A.; Amadelli, R., Photocatalysis with Organized Systems for the Oxofunctionalization of Hydrocarbons by O<sub>2</sub>. *Chem. Rev.* **2002**, *102*, 3811-3836.
47. (a) Suslick, K. S.; Watson, R. A., The photochemistry of chromium, manganese, and iron porphyrin complexes. *New J. Chem.* **1992**, *16* (5), 633-42; (b) Hennig, H., Homogeneous photo catalysis by transition metal complexes. *Coord. Chem. Rev.* **1999**, *182*, 101-123.
48. Zhang, R.; Newcomb, M., Laser Flash Photolysis Generation of High-Valent Transition Metal-Oxo Species: Insights from Kinetic Studies in Real Time. *Acc.Chem. Res.* **2008**, *41* (3), 468-477.
49. Zhang, R.; Harischandra, D. N.; Newcomb, M., Laser flash photolysis generation and kinetic studies of corrole-manganese(V)-oxo intermediates. *Chem. Eur. J.* **2005**, *11* (19), 5713-5720.
50. (a) Zhang, R.; Huang, Y.; Abebrese, C.; Thompson, H.; Vanover, E.; Webb, C., Generation of trans-dioxoruthenium(VI) porphyrins: A photochemical approach. *Inorg.*

*Chim. Acta* **2011**, 372, 152-157; (b) Zhang, R.; Vanover, E.; Luo, W.-L.; Newcomb, M., Photochemical generation and kinetic studies of a putative porphyrin-ruthenium(V)-oxo species. *Dalton Transactions* **2014**, 43, 8749-8756.

51. Lindsey, J.; Wagner, R. D., Investigation of the synthesis of ortho-substituted tetraphenylporphyrins. *J. Org. Chem.* **1989**, 54, 828-836.

52. Adler, A. D.; Longo, F. R.; Kampas, F. K., J., *J. Inorg. Nucl. Chem.* **1970**, 32, 2443-2445.

53. (a) Kwong, K. W.; Lee, N. F.; Ranburg, D.; Malone, J.; Zhang, R., Visible light-induced formation of corrole-manganese(V)-oxo complexes: Observation of multiple oxidation pathways. *J. Inorg. Biochem.* **2016**, 163, 39-44; (b) Lee, N. F.; Malone, J.; Jeddi, H.; Kwong, K. W.; Zhang, R., Visible-light photolysis of corrole-manganese(IV) nitrites to generate corrole-manganese(V)-oxo complexes. *Inorg. Chem. Commun.* **2017**, 82, 27-30.

54. Jeong, Y. J. K., Y.; Han, A.-R.; Lee, Y.-M.; Kotani, H.; Fukuzumi, S.; Nam, W., Hydrogen Atom Abstraction and Hydride Transfer Reactions by Iron(IV)-Oxo Porphyrins. *Angew. Chem., Int. Ed* **2008**, 47, 7321-7324.

55. (a) Kwong, K. W. P., D.; Malone, J.; Lee, N. F.; Kash, B.; Zhang, R., An investigation of ligand effects on the visible light-induced formation of porphyrin-iron(IV)-oxo intermediates. *New J. Chem.* **2017**, 41, 14334-14341; (b) Lee, N., F.; Patel, D.; Liu, H.; Zhang, R., Insights from kinetic studies of photo-generated compound II models: Reactivity toward aryl sulfides. *J. Inorg. Biochem.* **2018**, 183, 58-65.

56. Pan, Z.; Newcomb, M., Kinetics and mechanism of oxidation reactions of porphyrin-iron(IV)-oxo intermediates. *Inorg. Chem.* **2007**, 46, 6767-6774.

57. Zhang, R.; Horner, J. H.; Newcomb, M., Laser Flash Photolysis Generation and Kinetic Studies of Porphyrin-Manganese-Oxo Intermediates. Rate Constants for Oxidations Effected by Porphyrin-MnV-Oxo Species and Apparent Disproportionation Equilibrium Constants for Porphyrin-MnIV-Oxo Species. *J. Am. Chem. Soc.* **2005**, *127* (18), 6573-6582.
58. Machii, K. W., Y.; Morishima, I., Acylperoxo-Iron(III) Porphyrin Complexes: A New Entry of Potent Oxidants for the Alkene Epoxidation. *J. Am. Chem. Soc.* **1995**, *117* (25), 6691-6697.
59. Pan, Z.; Zhang, R.; Newcomb, M., Kinetic studies of reactions of iron(IV)-oxo porphyrin radical cations with organic reductants. *J. Inorg. Biochem.* **2006**, *100* (4), 524-532.
60. Groves, J. T.; Gross, Z.; Stern, M. K., Preparation and Reactivity of Oxoiron(IV) Porphyrins. *Inorg. Chem.* **1994**, *33* (22), 5065-72.
61. (a) Gross, Z.; Nimri, S., A Pronounced Axial Ligand Effect on the Reactivity of Oxoiron(IV) Porphyrin Cation Radicals. *Inorg. Chem.* **1994**, *33*, 1731-1732; (b) Urano, Y. H., T.; Hirobe, M.; Nagano, T., Pronounced Axial Thiolate Ligand Effect on the Reactivity of High-Valent Oxo-Iron Porphyrin Intermediate. *J. Am. Chem. Soc.* **1997**, *119*, 12008-12009.
62. Dolphin, D.; Traylor, T. G.; Xie, L. Y., Polyhaloporphyrins: Unusual ligands for metals and metal-catalyzed oxidations. *Acc. Chem. Res.* **1997**, *30* (251-259).
63. Pan, Z. N., M.; , Acid-catalyzed disproportionation of oxoiron(IV) porphyrins to give oxoiron(IV) porphyrin radical cations. *Inorg. Chem. Commun.* **2011**, *14* (6), 968-970.

64. Gross, Z. N., S.; Seeing the Long-Sought Intermediate in the Reaction of Oxoiron(IV) Porphyrin Cation Radicals with Olefins. *J. Am. Chem. Soc.* **1995**, *117* (30), 8021-8022.
65. Ghiladi, R. A. K., R. M.; Guzei, I.; Rheingold, A. L.; Neuhold, Y.-M.; Hatwell, K. R.; Zuberbuhler, A. D.; Karlin, K. D.;, (F8TPP)FeII/O<sub>2</sub> Reactivity Studies {F8TPP = Tetrakis(2,6-difluorophenyl)porphyrinate(2-)}: Spectroscopic (UV-Visible and NMR) and Kinetic Study of Solvent-Dependent (Fe/O<sub>2</sub> = 1:1 or 2:1) Reversible O<sub>2</sub>-Reduction and Ferryl Formation. *Inorg. Chem.* **2001**, *40* (23), 5754-5767.
66. Song, B. P., K.; Yu, B.;, *Korean Chem. Soc.* **1997**, *41*, 495-501.

## CURRICULUM VITAE

### EDUCATION

---

- M. Sc. in Chemistry: Western Kentucky University, 2016 – 2018
- B. Sc. in Chemistry and Biochemistry: Western Kentucky University, 2011 – 2015

### RESEARCH AND EXPERIENCE

---

- Graduate Research Assistant, Western Kentucky University, 2016 – 2018
  - Thesis: *Biomimetic Studies of Oxidation Reactions by Metalloporphyrins Through Ligand Effect and Kinetic Studies of Photo-Generated Porphyrin-iron(IV)-oxo, Compound II Models*
- Undergraduate Research Assistant, Western Kentucky University, 2015 – 2016
  - Honors Thesis: *Poly(3-hexylthiophene) Nanorods as a Donor for Organic Photovoltaics*

### AWARDS & HONORS

---

- Reserve Officers Assoc. of the US, 2017
  - Dr. Charles Hood Scholarship, 2017
  - WKU ROTC Room and Board Scholarship, 2016 – 2018
  - Guaranteed Reserve Force Duty Scholarship, 2016 – 2018
  - Undergraduate Organic Chemistry Award, WKU, 2014 – 2015
  - Sophia & Zuheir Scholars Scholarship, WKU, 2014 – 2015
  - Faculty-Undergraduate Student Engagement Grant, WKU, 2014 – 2015
  - Student Development Grant, SGA WKU, 2014 – 2015
  - Honors Development Grant, WKU, 2013 & 2014
  - College Heights Foundation Scholarship, WKU, 2013
  - Academic Excellence Award, Navitas at WKU, 2013
  - Outstanding Student Award, Navitas at WKU, 2013
-

## PEER-REVIEWED PUBLICATIONS

---

- Lee, N. F.; Patel, D.; Liu, H.; Zhang, R., Insights from kinetic studies of photo-generated compound II model: Reactivity toward arly sulfides. *J. Inorg. Biochem.*, **2018**, 183, 58-65
- Kwong, K. W.; Patel, D.; Malone, J.; Lee, N. F.; Kash, B.; Zhang, R., A investigation of ligand effect on visible light-induced formation of porphyrin-iron(IV)-oxo complexes. *New J. Chem.*, **2017**, 41, 14334-14341
- Patel, D.; Brown, D.; Sreeramulu, N. N.; Rathnayake, H., Preparation of semiconducting polymer nanorods by base-caalyzed covalent synthesis. *Science Adv. Today*. **2015**, 1, 25221

## PROFESSIONAL PRESENTATIONS

---

- Patel, D.; Zhang, R., “Biomimetic Studies of Oxidation Reactions by Metalloporphyrins Through Ligand Effect and Kinetic Studies of Photo-Generated Porphyrin-Iron(IV)-Oxo Compound II Models.” 48<sup>th</sup> Annual WKU Student Research Conference (2018), Bowling Green, KY.
- Patel, D.; Malone, J.; Kwong, K. W.; Zhang, R., “Photochemical Generation and Kinetic Studies of High Valent Iron(IV)-oxo Porphyrins.” 47<sup>th</sup> Annual WKU Student Research Conference (2017), Bowling Green, KY.
- Patel, D.; Rathnayake, H., “Poly(3-hexylthiophene) Nanorods as a Donor for Organic Photovoltaics.” American Chemical Society (2015), Denver, CO.
- Patel, D.; Neesu, R.; Sreeramulu, N. N.; Huzyak, P.; Ferguson, J.; Sharpsteen, J.; Rathnayake, H.; “Donor-Acceptor Nanostructures for Energy Harvesting.” Poster at the Capitol (2015), Frankfort, KY.
- Patel, D.; Neesu, R.; Rathnayake, H.; “Fused Arenes-based Molecular Systems as Additives for Organic Photovoltaics.” Kentucky Academy of Sciences (2014), Lexington, KY.
- Patel, D.; Rathnayake, H.; “Carbon-based Nano-material for Green Technology.” Kentucky Honors Roundtable (2014), Bowling Green, KY.
- Patel, D.; Brown, D.; Rathnayake, H.; “Poly(3-hexylthiophene) Nanorods as a Donor

for Organic Photovoltaics.” American Chemical Society (2014), Dallas, TX.

- Patel, D.; Brown, D.; Rathnayake, H.; “Poly(3-hexylthiophene) Nanorods as a Donor for Organic Photovoltaics.” Kentucky Academy of Sciences (2013), Morehead, KY.

## **CERTIFICATIONS**

---

- Federal Emergency Management Agency (FEMA)
- Introduction to the Incident Command System (ICS100) (2017)
- ICS for Single Resources and Initial Action Incident (ICS-200) (2017)
- Department of Defense (DOD) Fire and Emergency Services Certification Program
- Hazardous Materials Awareness (2016)
- Hazardous Materials Operations (2016)
- Hazardous Ops – Mass Decontamination (2016)
- Hazardous Ops – Personal Protective Equipment (2016)

## **EXTRA-CURRICULAR ACTIVITIES**

---

- Kentucky Science Olympiad Volunteer 2016/2017
- Chair of Finance of Indian Student Association (ISA), Western Kentucky University, 2016-2018
- International Student Diplomat – Western Kentucky University 2014-2015
- Super Saturdays Aid for 4<sup>th</sup> and 5<sup>th</sup> graders: 2013 – 2015
- Donations to the Humane Society 2013 – 2014
- Volunteer for the Bowling Green International Festival 2012 – 2016
- Volunteer for Habitat for Humanity 2011-2013
- American Cancer Society (Relay for Life) – 2012



## ABBREVIATIONS AND SYMBOLS

---

Ar	Aryl
BF <sub>3</sub> ·OEt <sub>2</sub>	Boron trifluoride diethyl etherate
CYP450s	Cytochrome P450 enzymes
DDQ	2,3-Dichloro-5,6-dicyano- <i>p</i> -benzequinone
DMF	<i>N,N</i> -Dimethylformamide
Fe <sup>III</sup> (Por)Cl	Iron(III) porphyrin complex
Fe <sup>III</sup> (TPP)Cl	Iron(III) 5,10,15,20-tetraphenylporphyrin chloride
<sup>1</sup> H-NMR	Proton nuclear magnetic resonance
H <sub>2</sub> TPFPP	5,10,15,20-Tetrakis(pentafluorophenyl)porphyrin
H <sub>2</sub> TDFPP	5,10,15,20-Tetrakis(2,6-difluorophenyl)porphyrin
HPLC	High-performance liquid chromatography
<i>k</i> <sub>0</sub>	Background rate constant
<i>k</i> <sub>ox</sub>	Second-order rate constant
<i>k</i> <sub>obs</sub>	Observed pseudo-first-order rate constant
<i>k</i> <sub>rel</sub>	Relative rate constant
LFP	Laser flash photolysis
<i>m</i> -CPBA	<i>meta</i> -Chloroperoxybenzoic acid
NADH	Nicotinamide adenine dinucleotide
NADPH	Nicotinamide adenine dinucleotide phosphate
OAT	Oxygen atom transfer
PhI(OAc) <sub>2</sub>	Iodobenzene diacetate
ppm	Parts per million

Sub	Substrate
TLC	Thin layer chromatography
TMS	Tetramethylsilane
UV-vis	Ultraviolet-visible

---